The Astronomical Journal, 153:172 (23pp), 2017 April https://doi.org/10.3847/1538-3881/aa64dc

Forming the Flora Family: Implications for the Near-Earth Asteroid Population and Large Terrestrial Planet Impactors

David Vokrouhlický[1], William F. Bottke[2], and David Nesvorný[2]
[1] Institute of Astronomy, Charles University, V Holešovičkách 2, CZ–18000 Prague 8, Czech Republic; vokrouhl@cesnet.cz
[2] Department of Space Studies, Southwest Research Institute, 1050 Walnut Street, Suite 300, Boulder, CO 80302, USA
Received 2017 February 5; revised 2017 March 3; accepted 2017 March 4; published 2017 March 23

Abstract

Formed from a catastrophic collision of a parent body larger than 150 km in diameter, the Flora family is located in the innermost part of the main belt near the ν_6 secular resonance. Objects in this region, when pushed onto planet-crossing orbits, tend to have relatively high probabilities of striking the Earth. These factors suggest that Flora may be a primary source of present-day LL chondrite-like NEOs and Earth/Moon impactors. To investigate this possibility, we used collisional and dynamical models to track the evolution of Flora family members. We created an initial Flora family and followed test asteroids 1 and 3 km in diameter using a numerical code that accounted for both planetary perturbations and nongravitational effects. Our Flora family members reproduce the observed semimajor axis, eccentricity, and inclination distributions of the real family after $\simeq$1 to 1.4 Gyr. A consistency with the surface age inferred from crater spatial densities found on (951) Gaspra may favor the latter age. Our combined collisional and dynamical runs indicate that the family has lost nearly 90% of its initial kilometer-sized members. At its peak, 100–300 Myr after the family-forming event, Flora family members filled NEO space with nearly 1000 $D \geqslant 1$ km size bodies before fading to its present contribution of 35–50 such NEOs. Therefore, it is not currently a major source of large NEOs. We also find 700–950 and 35–47 kilometer-sized asteroids struck the Earth and Moon, respectively, most within the first 300 Myr after family formation. These results imply that Flora played a major role in providing impacts to the mid-Proterozoic Earth.

Key words: minor planets, asteroids: general

1. Introduction

The Flora asteroid family, which resides in the innermost region of the main asteroid belt, has been known for nearly a century. Curiously, our understanding of its properties has remained fairly murky even as our knowledge of the asteroid belt has increased. The key problems are that this family is probably old, its members are distributed widely in semimajor axis, eccentricity, and inclination space, and it is located in the middle of a zone crisscrossed by dynamical resonances than can affect the long-term evolution of the bodies. Hence, solving the puzzle of the Flora family, as Sherlock Holmes might say, is a "three pipe problem."

Historically, Hirayama found the Flora cluster shortly after his pioneering work that identified the Koronis, Eos, and Themis clusters from the limited data set of 790 orbits available to the author at that time (Hirayama 1918, 1919). In later papers, Hirayama provided details of how the proper semimajor axes, eccentricities, and inclinations of asteroid orbits could be used to map the Flora family in greater detail (e.g., Hirayama 1922). By 1928, the tabulated Flora family had the largest number of members out of all the known families, 63 out of a sample of 1025 asteroids with proper elements, but it was also recognized to be one of the most dispersed in proper elements (Hirayama 1928). Later work by Brouwer (1950) confirmed these characteristics, but he also used the orbital distribution of Flora family members to propose that the collisional disruption of parent body ejected the known fragments away at high velocities of $\simeq$300–500 m s^{-1}. These values were slightly lower than those calculated by Hirayama (1928), perhaps because Brouwer had used more accurate proper elements.

Given this wide dispersal, it was inevitable that some would look for sub-clusters in the Flora family. In fact, using a new sample of 1537 asteroid proper elements, Brouwer (1951) extended the Flora population to 125 objects and proposed an ensemble of four nearly intermixed sub-clusters named Flora I to IV. Unfortunately, the main tool he used to identify these sub-clusters, namely similar values of the secular angle $\varpi + \Omega$ (the sum of the longitudes of perihelion and node), was not correct. These clustered orbit angles are mainly influenced by the secular z_1 secular resonance, and do not belong to a separate physical cluster (an even more striking example of this misunderstanding was the analysis of the Eos family; see Vokrouhlický et al. 2006b). As fate would have it, his outermost Flora IV group may indeed contain more objects from the nearby and partially overlapping Baptistina family than the Flora family itself (see, e.g., Bottke et al. 2007; Parker et al. 2008; Masiero et al. 2012).

Regardless, this study opened Pandora's Box, with numerous subsequent studies partitioning the Flora population into different unrelated parts. The history of the Flora family from that time forward has lurched between two camps: one arguing for a single, collisionally born family and a second for several independent yet overlapping clusters formed by multiple disruption events. A useful review of pre-1990s studies for the Flora family may be found in the Asteroids and Asteroids II books (Gradie et al. 1979; Kozai 1979; Chapman et al. 1989; Valsecchi et al. 1989).

In most scientific problems, additional data helps to clarify the problem. The advent of advanced near-Earth object (NEO) surveys, and the subsequent rapid increase in main-belt asteroid discoveries in the 1990's, however, has been both a blessing and a curse for Flora family studies. The number of known inner main-belt asteroids has grown by an order of magnitude

or more since the early 1990's, but this has also made it more difficult to discern individual families, especially one as large and distributed as the Flora family, using an objective clustering method in the 3D space of proper orbital elements. The evolution of this problem is nicely documented in the seminal papers by the Italian-French group led by Zappalà et al. (1990, 1994, 1995). In the last paper of this series, Flora is proposed to be a clan, or a large subgroup, within a high concentration zone of asteroids that contains several substructures.

The question of whether one can objectively define Flora as a single dynamical family, defined as a statistically significant cluster in proper element space, was recently explored by Milani et al. (2014). At the time of this paper, the database of high-quality synthetic proper orbital elements had increased to 336 319, of which 115 000 resided in the low-inclination part of the inner main belt. Note that as an aside, current counts are >50% larger. Because the volume of the inner main-belt zone in proper element space is limited, even a random distribution of this number of proper elements will produce a high density of background asteroids. The objective and automatic clustering methods used on this problem will therefore only tend to reveal small compact clusters near the statistical noise level of the background. This identification problem is compounded by the fact that any large family hundreds of megayears old within the Flora zone will dynamically spread into a broad area by the diffusive effect of a dense overlapping collection of weak mean-motion resonances (e.g., Nesvorný & Morbidelli 1998; Morbidelli & Nesvorný 1999; Nesvorný et al. 2002b). Accordingly, the existence of a single spread-out family is difficult to discern using objective methods; at best, they can only help one identify the main group as a prospective clan.

To make further progress on the Flora family, one must look to other kinds of data that can provide us with additional telltale clues. Fortunately, we now have an abundance of data on prospective Flora family members from ground- and space-based observation surveys. For example, the Sloan Digital Sky Survey (SDSS) provided broadband photometric colors for more than 100 000 identified moving solar system objects, for most part main-belt asteroids (e.g., Parker et al. 2008; Masiero et al. 2015). Similarly, the *Wide-field Infrared Survey Explorer* (*WISE*) spacecraft has provided the means to compute geometric albedos (p_V) for more than 100 000 main-belt asteroids (e.g., Masiero et al. 2013, 2015). Additionally, it is also useful to bring in studies of asteroid absolute magnitude values (H) or diameters D to evaluate families. In family-forming events via collisonal disruption or cratering, the ejecta that can be observed tends to have a specific and recognizable pattern in semimajor axis versus H, or D, space (e.g., Vokrouhlický et al. 2006a). Collectively, these data sets provide us with intriguing evidence that the Flora family is not a set of sub-clusters but instead is a single large inner main-belt family (e.g., Dykhuis et al. 2014; Masiero et al. 2015; Nesvorný et al. 2015).

Additional evidence for a single large Flora family comes from the derived spin axis orientations of its members. According to dynamical evolution models of the Flora family (see Nesvorný et al. 2002b, or this paper), small family members with the largest semimajor axes should have reached those distances via Yarkovsky thermal drift forces. To reach these distances, however, the bodies had pole orientations near 180°, which in turn maximizes the outward drift rates of the bodies (e.g., Bottke et al. 2006b; Vokrouhlický et al. 2015). For numerous prospective Flora family members, lightcurve observations are now available in sufficient quantities to determine the orientation of their spin axes or, at the least, constrain the sense of their rotation. A check of the member's obliquities furthest from the Sun by Hanuš et al. (2013), Kryszczyńska (2013), and Dykhuis et al. (2016) confirms that they have values near 180°.

If we assume that Flora is a single family, one can use a variety of dynamical methods to estimate its age. For example, using a numerical simulation of how family members evolved in both semimajor axis and spin pole, Hanuš et al. (2013) roughly estimated the Flora family formed 1 ± 0.5 Gyr ago (Ga). This age compares favorably with a 0.5–0.9 Ga estimate computed from a numerical model of how Flora family members dynamically disperse in proper eccentricity and inclination over time (no Yarkovsky evolution included; Nesvorný et al. 2002b). A similar age of 950^{+200}_{-170} Myr was obtained by comparing the outermost extension of the family in the semimajor axis to the maximum values expected from bodies evolving by the Yarkovsky drift (Dykhuis et al. 2014; see also Brož et al. 2013).

An alternative method to find Flora's age can be obtained from modeling the crater population observed on (1272) Gaspra, a Flora family member and the first asteroid observed by the *Galileo* spacecraft. Presumably, Gaspra's surface age, or at least the age of its oldest craters, are the same age as the Flora family formation event. Using models of the crater production rate and how small craters evolve on its surface, estimates for Gaspra's surface age in the literature range from hundreds of megayears to gigayears (e.g., Greenberg et al. 1994; Chapman 1996; O'Brien et al. 2006; Marchi et al. 2015). Much of the wide spread comes from estimates made during the pioneering days of asteroid in situ research when the size frequency distribution of small, crater-forming projectiles was extremely uncertain. The latest results from the Dawn mission to Vesta, however, indicate crater spatial densities on Gaspra are only modestly higher than those found on or near the ∼500 km diameter basin Rheasilvia, whose superposed crater model age is ∼1 Ga (Marchi et al. 2014, 2015). This led Marchi et al. (2014, 2015) to compute a surface age for Gaspra of ∼1.5 Ga. This value is modestly larger but reasonably close to the ages reported by the dynamical methods discussed above.

In order to complete a tour of suggested ages for the Flora family, we mention the work of Kryszczyńska et al. (2012), who presented results from a large observational campaign to obtain rotation rates of Flora members. Near uniformity of the rotation rates for asteroids smaller than ≃5–10 km requires and age of at least a couple of hundreds of megayears in order to complete their relaxation by the nongravitational YORP torque effect (see also Pravec et al. 2008). Kryszczyńska et al. (2012) also noted that the spin-rate uniformity does not reach sizes observed in the Koronis family, about 2.5–3 Gyr old, suggesting that the Flora family is somewhat younger.

A key aspect of large families residing close to main-belt escape hatches is their ability to act as sources of both meteorites and large near-Earth asteroids (NEAs) delivered to Earth. In this paper, we are especially concerned about the latter, namely whether the Flora family has been a potential source of multi-kilometer-size NEAs in the past and what is its input into the current population. The Flora family is of particular interest because it resides next to the ν_6 secular

resonance. It has been shown that objects entering the ν_6 resonance efficiently feed the steady-state NEA population (e.g., Bottke et al. 2002a; Granvik et al. 2016). All things being equal, the ν_6 resonance is also much better than nearly any other powerful resonance at producing Earth/Moon impactors (e.g., Gladman et al. 1997; Morbidelli & Gladman 1998; Zappalà et al. 1998; Bottke et al. 2006a). Accordingly, this predicts that a large Flora family may have been a prolific source of large impacts on the terrestrial planets, with possible implications for the evolution of life on the Precambrian Earth.

An unsolved problem is the timing and magnitude of a Flora family member striking the Earth and terrestrial planets. Obtaining these values not only depends on the age of the Flora family but how long the family members take to evolve into nearby main-belt escape hatches. Previous estimates of the timing assumed the fragments were directly injected into the ν_6 resonance, which in turn led to an Earth impact shower lasting $\simeq$30 Myr after the family-forming event (Zappalà et al. 1998). The problem with this assumption, as we will show below, is that the Flora family-forming event probably did not directly inject any kilometer-size objects into the ν_6 resonance. Instead, the dominant process of transporting Flora fragments to the ν_6 resonance and other nearby escape hatches is Yarkovsky-driven semimajor axis drift. It causes Flora members to move toward smaller semimajor axis values, where they can enter the ν_6 resonance and become NEAs, or it helps them slowly walk into weak mean-motion resonances with Mars and Jupiter that take them to Mars-crossing orbits, where they again eventually turn into NEAs. Both processes operate over long timescales. This means that the Flora family may be contributing NEAs and planet impactors many hundreds of megayears after its formation. One of the main goals of our paper is to determine this exact impact profile in time.

We also want to determine how the Flora family's contribution to the NEA population quantitatively compares to the overall replenishment of NEAs with time and to the overall flux of large planetary impacts from the main belt. To answer these questions, we not only need a good model of the flux of Flora fragments escaping the main belt over time but also how to calibrate it in terms of the number of expected objects. Here again we have the advantage over the work of Zappalà et al. (1998) because current knowledge of multi-kilometer diameter bodies in the Flora family is much more precise than what was known nearly 20 years ago.

In this paper, we will first briefly review the Flora family data needed for our modeling work (Section 2). Next, in Section 3, we will introduce the numerical tools we will use to model the dynamical evolution of a synthetic Flora family since its formation. In Section 4, we will present results from our simulations and will estimate an age for the family by comparing our model family distribution in proper element space to observations. Next, we use our constrained model to predict the time evolution of Flora's contribution to the NEA population and the likely flux of impactors striking the terrestrial planets. Finally, in Section 5, we discuss the implications of our results.

2. Family Data

Over all of the possible aspects by which Flora family members could be characterized, we are mainly interested in two: (1) an estimate of the number of Flora members with diameter $D \geqslant 1$ km, defined here as $N(1)$, or $D \geqslant 3$ km, defined here as $N(3)$, and (2) a distribution of family members in proper orbital element space. Because the latter also depends on the cutoff diameter used for family members, and $D \geqslant 1$ km is currently observationally incomplete, we will use $D \geqslant 3$ km to investigate (2).

Concerning our family population, we use data from Masiero et al. (2013; see also Masiero et al. 2015), who analyzed main-belt families and their albedos using the rich data set provided by the *WISE* spacecraft. For Flora, they provide a population estimate of $D \geqslant 3$ km bodies of $N(3) \simeq 700$–900 that should be nearly complete. At this size, the slope of cumulative $N(D)$ distribution was estimated to -2.59 ± 0.03. Given that the $D \geqslant 1$ km bodies are observationally incomplete, we extrapolate this slope and get an approximate number of $N(1) \simeq 11\,600$–$16\,000$ for current Flora members. We consider this range to be a nominal assumption throughout this paper. However, should the size distribution slope between $D = 1$ and 3 km change to -2, say, the recalibrated $N(1)$ values would be smaller by a factor of $\simeq$1.9. Our estimates of Flora contribution to the near-Earth asteroid population and projectiles onto terrestrial worlds with 1 km size in Section 4 would change by the same factor.

We also note that Masiero et al. (2013) derived a mean geometric albedo for Flora family members to be $\simeq$0.29 with a standard deviation of $\simeq$0.09. Moreover, in their data, the tail of family members extends to albedo values as low as $\simeq$0.2. Unlike their size determinations, these albedo values should be taken with considerable caution. Pravec et al. (2012) studied systematic effects in the determination of small asteroid absolute magnitudes and found a mean offset of roughly $(-0.2, -0.4)$ in commonly used databases (e.g., Minor Planet Center, Lowell, Pisa). This means the mean albedo of Flora members should probably be shifted downward to $\simeq$0.25.

As to the structure of the family in proper element space, we use information from the nominal Flora family identification data set located at the NASA Planetary Data System (PDS) website at http://sbn.psi.edu/pds/resource/nesvornyfam.html (see also Nesvorný et al. 2015). This file contains 13 786 entries, but special care is needed to account for the existence of the largely overlapping Baptistina family in the same orbital element zone (e.g., Bottke et al. 2007; Dykhuis et al. 2014). Fortunately, the two families may be separated using the albedo and SDSS colors. We find that slightly more than 2 600 asteroids in the Flora family file at PDS have albedo values determined by *WISE*. Of these, more than 2 000 have geometric albedos larger than 0.18, a reasonable demarcation line to separate them from Baptistina members (see also data in Masiero et al. 2013). We consider these bodies safe members of the Flora family. These asteroids are shown in Figure 1 projected onto the plane of proper semimajor axis versus absolute magnitude. The solid gray line is defined by $H = 5 \log[(a - a_8)/C]$, where $a_8 = 2.2014$ au is the proper semimajor axis of (8) Flora and $C = 2 \times 10^{-4}$ au. This was defined as a V-shape boundary line of the Flora family in Dykhuis et al. (2014), and it shows that our definition and theirs are similar.

The small Flora family members in Figure 1 show a larger spread of semimajor axis values than larger family members. This is due to a combination of their larger initial ejection speed and their faster drift rates via the Yarkovsky effect (e.g., Vokrouhlický et al. 2006a). The horizontal slice, delimited by the gray dashed lines, illustrates where asteroids of $D = 3$ km

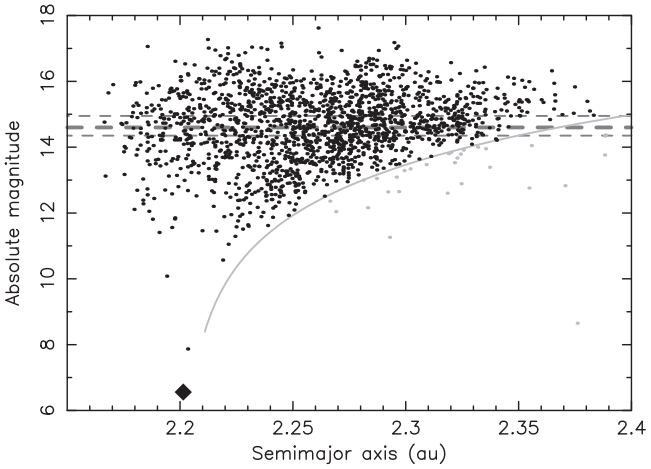

Figure 1. Known Flora family members with *WISE* albedo values $\geqslant$0.18. The diamond symbol indicates the position of (8) Flora, the largest member in the family. The smaller black circles show nominal family members. The gray circles are formal members found in the PDS family file that are deemed interlopers; they are too large for their relative distance in semimajor axis with respect to (8) Flora. Flora-family members that would reach semimajor axes smaller than $\simeq$2.15 au, either initially or in the course of time, were driven by the ν_6 resonance onto planet-crossing orbits. The thick dashed gray line shows absolute magnitude of $D = 3$ km size members for the mean geometric albedo of 0.29; the thinner gray lines are for albedo values $\pm$0.09 away from the mean, the observed dispersion of the Flora values (Masiero et al. 2013). The solid gray line represents a Yarkovsky thermal drift-inspired boundary curve for the Flora family from Dykhuis et al. (2014).

are statistically located given the range of geometric albedo values determined by Masiero et al. (2013). This subset of Flora members is used in our numerical experiments below because it is essentially observationally complete and it specifies where the $D \simeq 3$ km size asteroids are distributed in proper orbital element space. For instance, data in Figure 1 indicate that the semimajor axes of these asteroids range from $\simeq$2.16 au to $\simeq$2.36 au in a nonuniform way. Most members of this size reside between $\simeq$2.26 au and $\simeq$2.32 au, where they contribute to an overabundance of Flora members with larger semimajor axis values than (8) Flora or the largest family members (see also Figure 6). This configuration, half of a classical "V" shape (e.g., Bottke et al. 2006b; Vokrouhlický et al. 2015), is the characteristic "ear" produced by family members undergoing Yarkovsky and YORP evolution (for more details and examples, see Vokrouhlický et al. 2006a).

With the $D = 3$ km subset of Flora members identified, we can now determine their distribution in both proper eccentricity and sine of the inclination (e.g., Figures 7 and 8 below). Their mean values are 0.137 and 0.088, respectively, with a variance of 0.015 in both values. Note that these variances are unusually large, such that it has already been discussed in some detail by Nesvorný et al. (2002b). Calculating the characteristic velocity distance using proper elements (e.g., Zappalà et al. 1990), the individual changes in eccentricity and inclination needed to equal the variance over the $D = 3$ km members would be $\simeq$430 m s^{-1}. This value is much larger than the estimated escape velocity from the Flora-family parent body, some (80–100) m s^{-1} for a body of $\simeq$150–160 km in size (e.g., Brož et al. 2013). Additionally, the "rounded shape" of the eccentricity and inclination distributions is inconsistent with that formed by a family's initial velocity field (e.g., Carruba & Nesvorný 2016). Instead, it seems more likely that the semimajor axis, eccentricity, and inclination distributions in the Flora family have experienced substantial dynamical evolution.

3. Model

Here we describe the initial conditions and numerical model used to track the evolution of a synthetic Flora family after it was created in a disruption event. To do this job efficiently, we employed the well-tested numerical code `swift`[3] modified to include nongravitational effects as described in Section 3.2. Gravitational perturbations from the planets Mercury through Neptune were also included. We followed tens of thousands of test asteroids for 1 Gyr using a short three-day numerical timestep. To deal with the computational burden, we split our runs onto a large number of computer CPUs. The total time used was approximately eight months of wall clock time.

The orbital motion of the synthetic Flora asteroids was followed until they hit the Sun, one of the planets was effectively ejected from the inner solar system by a close encounter with Jupiter and reached a heliocentric distance of 1 000 au, or 1 Gyr of simulation time was reached. The elimination of bodies by solar impacts was set at a heliocentric distance of 0.05 au, about 10 solar radii. This value is rather restrictive, but it was imposed to prevent the orbits from reaching extreme perihelia values that might be mishandled by `swift`.

Typical families evolving by the Yarkovsky/YORP effects show a "V" shape in (a, H) and two prominent ears, while the observed Flora family in Figure 1 only shows the right ear. We infer from this that the left ear has been lost via dynamical evolution. The principal escape route is the adjacent ν_6 secular resonance that marks the innermost region of the main asteroid belt. Numerous simulations indicate that about (1.5–2)% of the bodies entering the ν_6 resonance hit the Earth and Venus, and about half of that percentage hit Mars (e.g., Morbidelli & Gladman 1998; Zappalà et al. 1998; Bottke et al. 2006a). Thus, by starting each Flora simulation with 10 000 Flora members, we expect to find 70–90 impacts on both Earth and Venus, and about half as many on Mars. This value is large enough that we have reasonable confidence that we will be able to discern the impact history of Flora family members. In addition, we also combined results from our twin simulations with slightly different initial conditions as described below in Section 3.1.

In order to model the orbital evolution of Flora family members, and in particular how this family feeds the population of asteroids on planet-crossing orbits, we need to include nongravitational effects in our simulations (see Section 3.2). We keep them on throughout the whole span of our simulations, even when our family asteroids leave the main-belt zone, though their role is minimized in the planet-crossing zone by the gravitational perturbations of terrestrial planets.

3.1. Initial Data

A possible complication in setting up our simulations is that we do not know when the Flora-family breakup took place. To deal with this issue, we considered the following steps.

First, we numerically integrated the nominal orbit of (8) Flora forward in time for 1 Myr. The initial MJD epoch

[3] *Software:* http://www.boulder.swri.edu/~hal/swift.html.

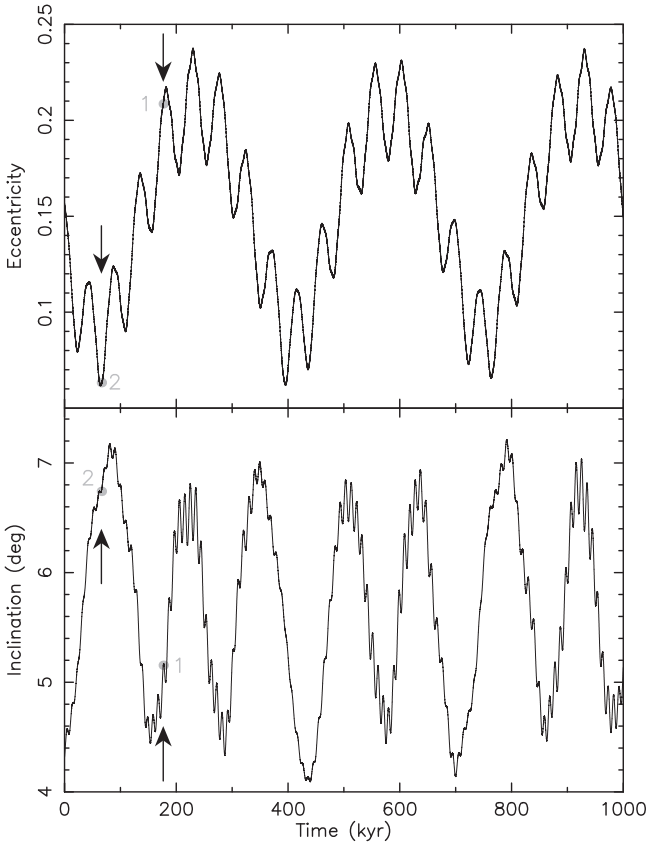

Figure 2. Orbit evolution of (8) Flora over a 1 Myr timescale: (top) eccentricity and (bottom) inclination with respect to the invariable plane of the solar system. The largest-amplitude effects in both elements are driven by secular interactions with Saturn's perihelion and node, respectively. The arrows point to two epochs, 1 and 2, chosen as initial conditions of our numerical integrations for our synthetic Flora family members.

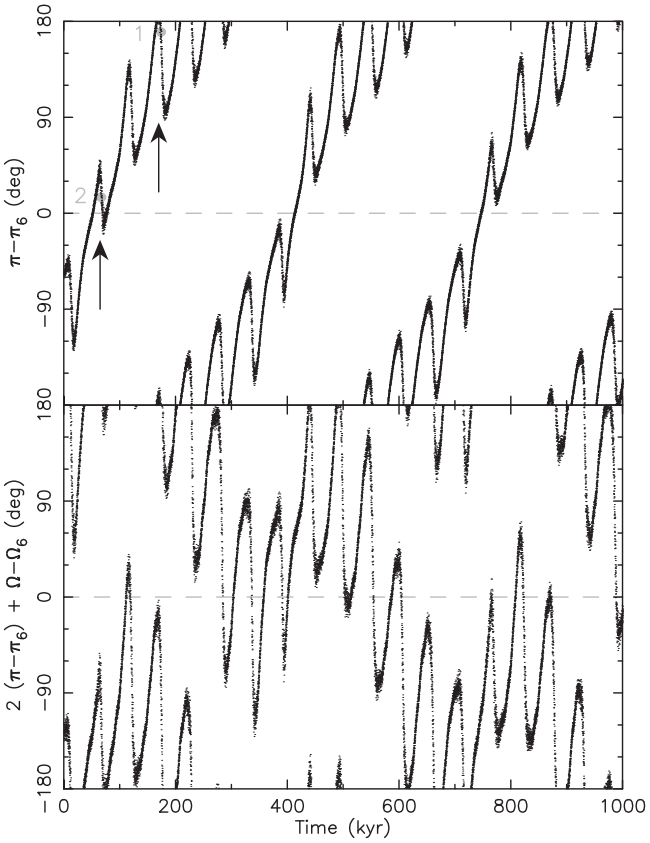

Figure 3. Behavior of resonance angles of (top) the ν_6 resonance and (bottom) the z_2 resonance in the orbit evolution of (8) Flora. Flora is not located in either of the two resonances, but the very slow circulation of these angles indicate a close proximity to both resonances. They play an important role in the long-term evolution and fate of Flora-family members as revealed in the numerical simulations discussed in Section 4. The arrows at the top panel point to two epochs, 1 and 2, chosen as initial conditions (compare with Figure 2). As expected, the minimum eccentricity corresponds to $\varpi - \varpi_6 \simeq 0^\circ$ (case 1 data), and the maximum eccentricity corresponds to $\varpi - \varpi_6 \simeq 180^\circ$ (case 2 data).

was 57000.0. The heliocentric position and velocity vector at this epoch was taken from the AstDyS site (http://hamilton.dm.unipi.it/astdys/). The planetary state vectors were obtained from the JPL DE405 ephemerides file. At this stage, only gravitational perturbations from the planets were considered. Orbital elements of (8) Flora were output every 50 years.

Figure 2 shows the eccentricity and inclination results of (8) Flora with respect to the invariable plane of the solar system (i.e., the semimajor axis is stable, showing only short-period and small-amplitude variations over this short timescale). Both orbital elements undergo large secular oscillations due to the nearby prominent secular resonances ν_6 and ν_{16} (e.g., Morbidelli & Henrard 1991; Knežević et al. 1991). Indeed, the proper frequencies g and s of Flora, provided by the AstDyS website, yield (1) $g - g_6 \simeq 3.7$ arcsec yr^{-1}, and (2) $s - s_6 \simeq -9.1$ arcsec yr^{-1}. The first value corresponds to a period of ≃350 kyr and the latter to ≃140 kyr, the prominent periodicity terms in eccentricity and inclination seen in Figure 2. An even longer period of ≃800 kyr results from their linear combination $2(g - g_6) + s - s_6 \simeq -1.6$ arcsec yr^{-1}, which is the fundamental frequency combination of the nonlinear secular resonance z_2 (e.g., Milani & Knežević 1992, 1994). The slow variation in the amplitude of inclination oscillations reveals the influence of the z_2 resonance on the orbit of (8) Flora.

Figure 3 shows the resonant angles associated with both lowest-frequency terms. Their circulation means (8) Flora has not yet been captured in either of them. Many fragments launched from this asteroid, however, may be injected into or will eventually reach them through dynamical evolution (especially the closer z_2 resonance, as will be demonstrated in our simulations in Section 4).

Other than the role of relatively weak mean-motion resonances with the planets Mars and Jupiter, the primary way asteroids are removed from the vicinity of the Flora family and pushed onto planet-crossing orbits is by having them reach the ν_6 secular resonance. If the initial ejection velocity from the Flora parent body was high enough, direct emplacement close to the orbit of Mars may also play some role.

In order to explore the influence of initial conditions on the evolution of Flora family members, we chose two time epochs from our orbital propagation runs of (8) Flora. They both represent extreme cases in regards to the possibility that the fragments were directly emplaced into the principal escape routes mentioned above. These two cases are highlighted in Figure 2: (1) case 1 roughly corresponds to the situation where we have a minimum value of the osculating inclination and a maximum value of osculating eccentricity, and (2) case 2 roughly corresponds to the situation where we have a minimum value of osculating eccentricity and a maximum value of osculating inclination. Thus, in case 1, we can determine what

happens when the fragments are ejected onto orbits with low perihelia, while in case 2 we can probe the effect of injecting the fragments close to the core of the ν_6 resonance.

Accordingly, with (1) and (2), our main suite of numerical runs were performed twice, each time starting from different initial conditions. Note this technique was also used by Nesvorný et al. (2007), who studied the role of the Flora family as a possible source of ancient ordinary chondrite meteorites. Obviously, the assumption implicitly made here is that the orbit of (8) Flora, plausibly representing the orbit of the parent body of the Flora family, is long-term stable. In other words, we are selecting initial conditions from an orbital simulation starting at the current epoch, but we are assuming they represent initial data from roughly a billion years ago or more. We discuss this assumption in more detail in the Appendix below.

Next, we must make assumptions on how the fragments of the Flora-family parent body were initially distributed in orbital element space. These values are set by our choice for the relative velocity distribution of the fragments launched away from the parent body. Here again, some degree of simplification is needed, though the reader should bear in mind that our results are statistical in nature and do not depend on the orbital evolution of any single Flora fragment. We are assuming that many realizations of the Flora breakup, including the ones discussed here, essentially provide the same statistical results as the real event.

For simplicity, we will assume that the fragment ejection field is isotropic, which we believe is a reasonable zeroth order approximation (see, e.g., Michel et al. 2002). As supporting evidence that this assumption is valid, we point out that the fragments in observed very young asteroid families do not reveal substantial evidence for non-isotropy at ejection (e.g., Nesvorný et al. 2002a). In addition, we will assume the fragments were all ejected with the same representative velocity. In modeling many different asteroid families, we have found that the family formation event typically produces ejection velocities for multi-kilometer bodies comparable to the escape velocity of the parent body (e.g., Michel et al. 2002; Vokrouhlický et al. 2006a). For the Flora parent body, which was possibly $\simeq$150–160 km in diameter (e.g., Brož et al. 2013), the escape velocity was likely in the (80–100) m s^{-1} range. For our production simulations, we used 100 m s^{-1} as our ejection relative velocity value.

To set the orbits of the initial fragments, we have to assume the bodies were ejected at a particular moment during the parent body's revolution around the Sun. This means the fragments' relative positions not only depend on the argument of perihelion ω, set by the choice of epochs for case 1 or case 2, but also on the true anomaly f along the orbit. Our choice, indicated in Figure 4, avoids degenerate situations, such as $\omega + f \simeq 90^\circ$ collapsing all inclinations to a single value.

Finally, while we believe our initial velocity dispersion of 100 m s^{-1} is reasonably well justified, we also ran a limited suite of simulations using 300 m s^{-1} (Section 4.3). The motivation here was to determine the sensitivity of our results to this important parameter rather than considering them strictly realistic.

3.2. Nongravitational Effects Included

While the effects of gravitational perturbations from the planets on the heliocentric motion of small bodies are the primary function of the `swift` package, our work requires us to complement it by including the effects of nongravitational forces relevant to multi-kilometer-sized bodies. Specifically, our code includes Yarkovsky thermal drift forces; over long timescales, the Yarkovsky effect can add or subtract orbital energy to small asteroids and thus secularly change their semimajor axes (e.g., Bottke et al. 2006b; Vokrouhlický et al. 2015). This force is caused by sunlight; when asteroids heat up in the Sun, they eventually re-radiate the energy away as heat, which in turn creates a tiny thrust. This recoil acceleration is much weaker than solar and planetary gravitational forces, but it can produce substantial orbital changes over timescales ranging from millions to billions of years. This dynamical mechanism is the primary way small main-belt bodies are transported to resonances that can push them onto planet-crossing orbits.

In the case of Flora family members, escape from the main belt primarily means being pushed by the Yarkovsky effect into the nearby powerful ν_6 resonance that defines the inner edge of the main belt. For larger family members that drift very slowly, however, this can also mean becoming trapped into weaker mean-motion resonances with Mars and Jupiter that can also push them into Mars-crossing orbits. For the most part, smaller asteroids drift fast enough to jump these narrow resonances (e.g., Bottke et al. 2002b).

A twin phenomenon to the Yarkovsky effect is the Yarkovsky–O'Keefe–Radzievskii–Paddack (YORP) effect that can secularly modify the rotation rate and spin axis orientation of small asteroids. This thermal torque, also produced by the absorption and re-radiation of sunlight, cannot be neglected because the strength and direction of the Yarkovsky thermal forces depend on rotation rate and spin axis obliquity. Accordingly, a synthesis of both effects must be included to obtain realistic simulations of small-body orbital evolution.

Various implementations of the Yarkovsky and YORP effects within the `swift` package have been discussed in the literature over the past decade. It is not our intention to provide details here. Instead, we refer the reader to Granvik et al. (2017); it includes an extensive discussion of how these effects were treated in our simulations discussed below. Here we only provide a brief overview.

Unlike the gravitational effects of the Sun and the planets, models of the Yarkovsky and YORP effects depend on a number of physical parameters that are a priori unknown and must be assumed. As before, we rely on the principle that the statistical properties of a population of bodies, such as their distributions in orbital element space, are less dependent on the assumptions made than the orbital fate of the individual bodies. The main problem here is accurately treating the YORP effect; our nominal model does not yet account for (1) tumbling that would naturally occur when the body starts rotating very slowly (e.g., Vokrouhlický et al. 2007, 2015) or (2) rotational fission that would naturally occur when a kilometer-sized or larger body reaches a spin period of approximately 2–3 hr. Instead, as an approximation, our model imposes boundaries on YORP-driven rotation rate evolution and sets an empirical solution when these limits are reached.

The characteristic timescale for a YORP-driven asteroid to reach the boundaries from a nominal rotation rate ω_0, corresponding to $\simeq$(6–12) hr, is called the "YORP-cycle" timescale. It may be approximated with a few times $T_{\rm YORP} \simeq \omega_0/(d\omega/dt)_0$, where $(d\omega/dt)_0$ is a characteristic

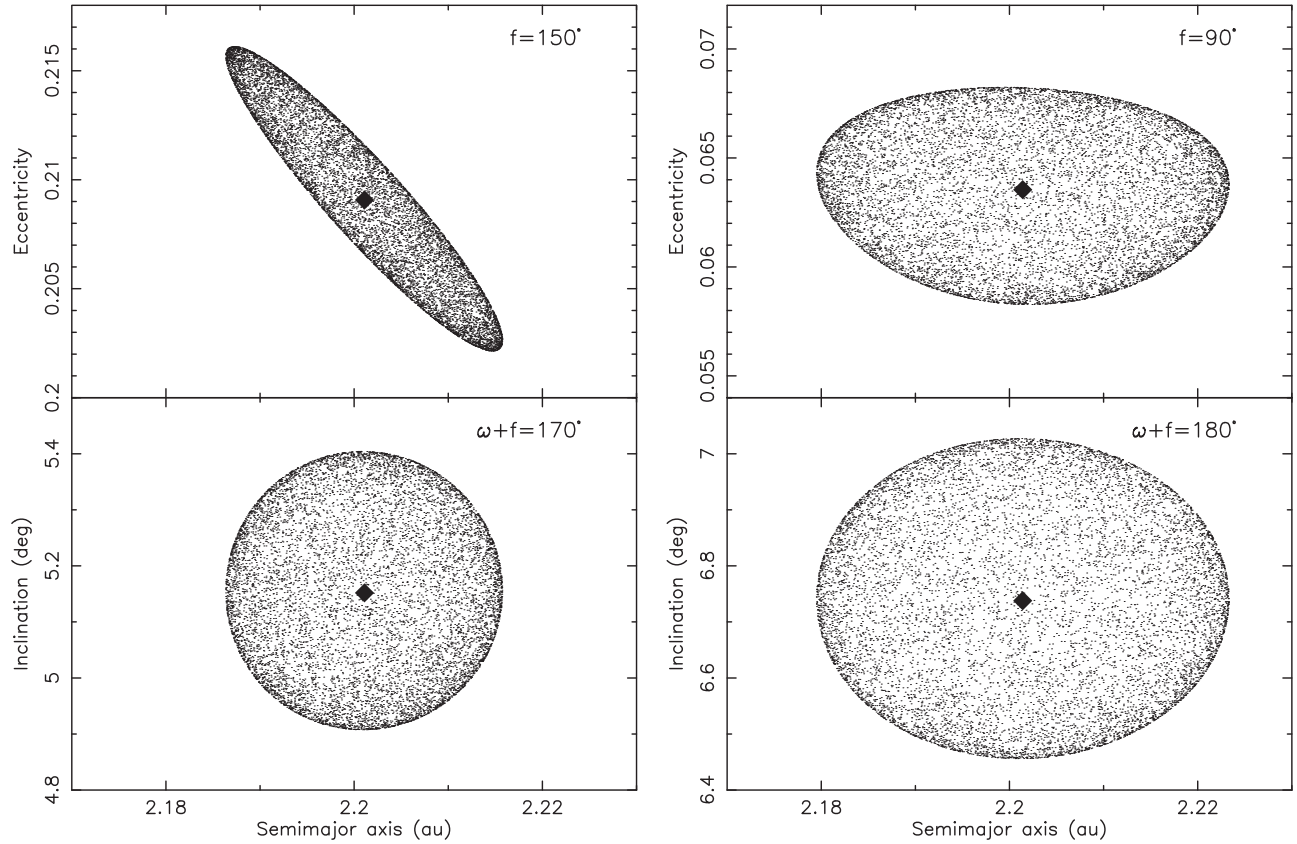

Figure 4. Initial values of the osculating orbital semimajor axis, eccentricity, and inclination for 10 000 fragments in our simulations that start at the case 1 epoch (left panels) and case 2 epoch (right panels). The labels indicate the values of the argument of perihelion ω and true anomaly f of the parent body when the breakup took place. These values are used in the Gauss equations to relate the positions of the fragments to the parent body position (black diamond).

rotation-rate secular change due to YORP. The complication is how to accurately model the orbital evolution of small members in moderately old families, including the Flora family, is that $T_{\rm YORP}$, and thus the YORP-cycle timescale is shorter than the age of the family. Consider that for $D = 3$ km bodies in the Flora family zone, $T_{\rm YORP} \simeq 25$–50 Myr (e.g., Čapek & Vokrouhlický 2004; Vokrouhlický et al. 2015).

Previously, nominal or "static" models of the YORP effect assume that the evolution of the obliquity and rotation rates would steadily change until an endstate like those described in (1) or (2) were reached. In careful studies of the YORP effect on synthetic asteroids, it was found that changes in the surface, such as a new crater being formed, a boulder moving around on the surface, or the asteroid shape morphing into a new configuration in response to the addition or subtraction of rotational angular momentum may lead to additional possibilities (see, e.g., Statler 2009; Bottke et al. 2015b; Cotto-Figueroa et al. 2015; Vokrouhlický et al. 2015). In practice, the evolution of the obliquity and rotation rate by the YORP effect becomes decoupled from one another. This is what is referred to as the "stochastic" YORP effect. Our discussion in the Appendix of Bottke et al. (2015b) provides the reader with some simple ways to understand this concept.

In the stochastic YORP model, the obliquity evolves as in the static YORP model, but the evolution of the rotation rate becomes slower; it effectively begins to undergo a random walk in response to all of the shape changes taking place on the asteroid. This extends the length of the YORP cycle. The primary empirical parameter is then the timescale $T_{\rm reset}$ to reset the surface properties of the body in regard to the strength of the YORP effect, or rather the ratio $\mathcal{R} = T_{\rm reset}/T_{\rm YORP}$. If $\mathcal{R} \gg 1$, we are back in the regime of the static YORP model; in the opposite limit $\mathcal{R} < 1$, one may explore the benefit of extending the YORP cycle timescale. In Section 4.2, we shall explore how the adjustment of $\mathcal{R}$ may help model the Flora family structure.

Additional remarks on the nominal parameters used for modeling the Yarkovsky and YORP effect are provided below.

Yarkovsky effect. The thermal acceleration applied to each Flora family member is modeled using formulas given in Vokrouhlický et al. (2000). They are based on a linearized heat-transfer solution for a spherical body. Only the diurnal variant is taken into account. The implied thermal relaxation timescale is much shorter than the orbital period about the Sun. Physical parameters needed to fully specify the Yarkovsky acceleration are (1) diameter D, (2) surface thermal inertia Γ, (3) rotation period P, (4) orientation of the spin axis $\boldsymbol{s}$, and (5) bulk density ρ. The size of Flora members for which we run our simulations is specified in Section 4. We set surface thermal inertia $\Gamma = 200\ {\rm J\,m^{-2}\ K^{-1}\ s^{-1/2}}$, appropriate for kilometer-size asteroids in the Flora region (e.g., Delbò et al. 2007, and updates from the first author). The bulk density is assumed to be $\rho = 2\ {\rm g\,cm^{-3}}$, also appropriate for small S-type asteroids in the Flora region (e.g., Carry 2012). The values of P and $\boldsymbol{s}$ are modeled in detail using the YORP effect.

YORP effect. Evolution of the asteroids' spin-state parameters $(P, \boldsymbol{s})$ is modeled using the symplectic propagator formulated by Breiter et al. (2005). With this, we also directly take into account the solar gravitational torque on $\boldsymbol{s}$ and the potentially complicated interplay of the induced regular

precession of $\boldsymbol{s}$ with the precession of the orbital plane of the body (see Vokrouhlický et al. 2006c; Vraštil & Vokrouhlický 2015, for specific analyses of bodies in the Flora region). For the YORP effect, we use the model developed in Čapek & Vokrouhlický (2004), including their estimate of the mean YORP torques computed for a sample of 200 Gaussian random spheres.

So far, our parameters are applicable to the static YORP approach. The stochastic YORP case, given a chosen $\mathcal{R}$ value, is modeled as described in Bottke et al. (2015b). As mentioned above, the stochastic YORP model provides a bridge between results from the static model ($\mathcal{R} \gg 1$ limit) to those where only the Yarkovsky accelerations with extreme values of obliquity were taken into account ($\mathcal{R} \ll 1$ limit). The boundary problem, namely the empirical procedure that the code uses when the rotation rate becomes too small (tumbling limit) or too large (fission limit), is treated as described in Bottke et al. (2015b) or Granvik et al. (2017).

To start a simulation, we need to specify initial conditions for $(P, \boldsymbol{s})$ of each Flora fragment and set several parameters. Note that information about likely distributions of $(P, \boldsymbol{s})$ in the aftermath of the Flora parent body breakup is limited. In large asteroid families, this information has been lost for smaller family members by subsequent evolution via the YORP effect. Computer simulations, such as those described in Michel et al. (2002), lack the resolution to tell us how to set these parameters, while laboratory experiments only provide results of fragmentation events on much smaller scales (e.g., Giblin et al. 1998; Holsapple et al. 2002). We thus opt again to use simple assumptions. First, the spin rates are chosen using a Maxwellian distribution of rotation rates $1/P$, with a maximum 8 hr rotation period and a dispersion corresponding to 3 hr. Second, the spin vector orientations $\boldsymbol{s}$ are selected from an isotropic distribution. Note that for kilometer-sized asteroids, the memory of these initial data are forgotten on a $T_{\rm YORP}$ timescale, so getting these values modestly incorrect is probably not a problem for our results.

The magnitude of the solar gravitational torque requires a value of dynamical ellipticity of each asteroid, namely $\Delta = [C + \frac{1}{2}(A + B)]/C$, where (A, B, C) are the principal moments of the inertia tensor. We assign Δ randomly from a Gaussian distribution with a 0.3 mean value and 0.1 variance. This matches reasonably well Δ values for small asteroids whose shapes have been determined (e.g., Vokrouhlický & Čapek 2002). It is also consistent with measurements of fragments from laboratory disruption experiments, though these bodies are much smaller than the fragments produced by a family-forming event (Giblin et al. 1998).

4. Results

As discussed in Section 3.1, we ran two sets of simulations of synthetic Flora family, each for one of the two chosen initial orbital conditions (cases 1 and 2). Each of these sets was performed for two asteroid sizes: $D = 1$ km and $D = 3$ km. By choosing different initial orbital conditions, we explored how the results depend on the (unknown) formation epoch of the family.

Our runs with two different asteroid sizes served a different purpose as well. In Section 2, we established the distribution of the observed Flora family in proper element space for $D \simeq 3$ km members, where presumably our knowledge of the family is nearly complete. Thus, in this situation, we do not need to worry about the role of observational biases. By running a suite of simulations for $D = 3$ km asteroids, we can directly compare our results with known Flora family members. In particular, we are interested in matching the fragment distributions in proper orbital elements. The population of $D = 3$ km asteroids among NEAs, however, is less numerous and therefore potentially subject to larger fluctuations compared to the $D = 1$ km population. In addition, some of the constraints discussed in Section 5 rely on the flux of approximately $D = 1$ km impactors. This motivates the use of $D = 1$ km asteroids in our simulations as well.

4.1. Nominal Simulations

Before presenting our most realistic simulations, we find it useful to compare and contrast two sets of simulations that do not match the Flora family's orbital structure constraints. They also help to set a context for the solutions discussed in Section 4.2.

In the first simulation set, we included the Yarkovsky effect but disregarded the rotation state dynamics of the Flora family members. Accordingly, we neglect the YORP effect, the effects of solar gravitational torques, and the inertial torques due to precession orbital planes. Additionally, Yarkovsky semimajor axis drift rates are maximized by assuming constant obliquity values of 0° or 180°; they are randomly assigned to the propagated bodies with equal probability. This test provides us with an approximation of how the Flora family formation event affected the NEA population. It was assumed that the properties of the current Flora family would not be reproduced.

Indeed, the left panels in Figure 5 show the normalized distributions of both the observed and simulated Flora family in the proper semimajor axis, eccentricity, and sine of inclination resulting from this simulation for $D = 3$ km family members. The data for the simulated family are shown at the beginning (0 Myr) and at the end (1 Gyr) of our simulation. Instead of computing exact synthetic proper eccentricities and sine of inclinations, according to the method of Knežević & Milani (2000), we simplified the procedure by computing the respective mean values over a running 5 Myr wide interval of time. We verified that the differences between these orbital mean values and the exact values of the synthetic proper elements typically differed by $\simeq$0.02 (for stable orbits in the main belt). This is much smaller than the extension of the Flora family that we would like to match.

The principal mismatch of this simulation is seen in the top left panel of Figure 5, where we show the final semimajor axis distribution. The initial synthetic family has a much narrower distribution than the observed family because the initial ejection speeds were 100 m s^{-1}. Within 0.5 Gyr, the fragments given obliquity values of 180° were eliminated through the ν_6 resonance. Those that were initially given obliquity values of 0° drift together toward larger semimajor axis values. At 1 Gyr, they reached a mean value of $a \simeq 2.35$ au, but the width of their distribution stayed the same as that of their initial distribution, which was set by the ejection velocity. A tail of lower semimajor axis values was due to several asteroids temporarily captured and then released in weak mean-motion resonances. The fact that at 1 Gyr the asteroids drifting outward at maximum speed reached the observed border of the Flora family suggests that this value is close to the family's minimum age (see Dykhuis et al. 2014). Note, however, that our goal is to match the entire semimajor axis distribution.

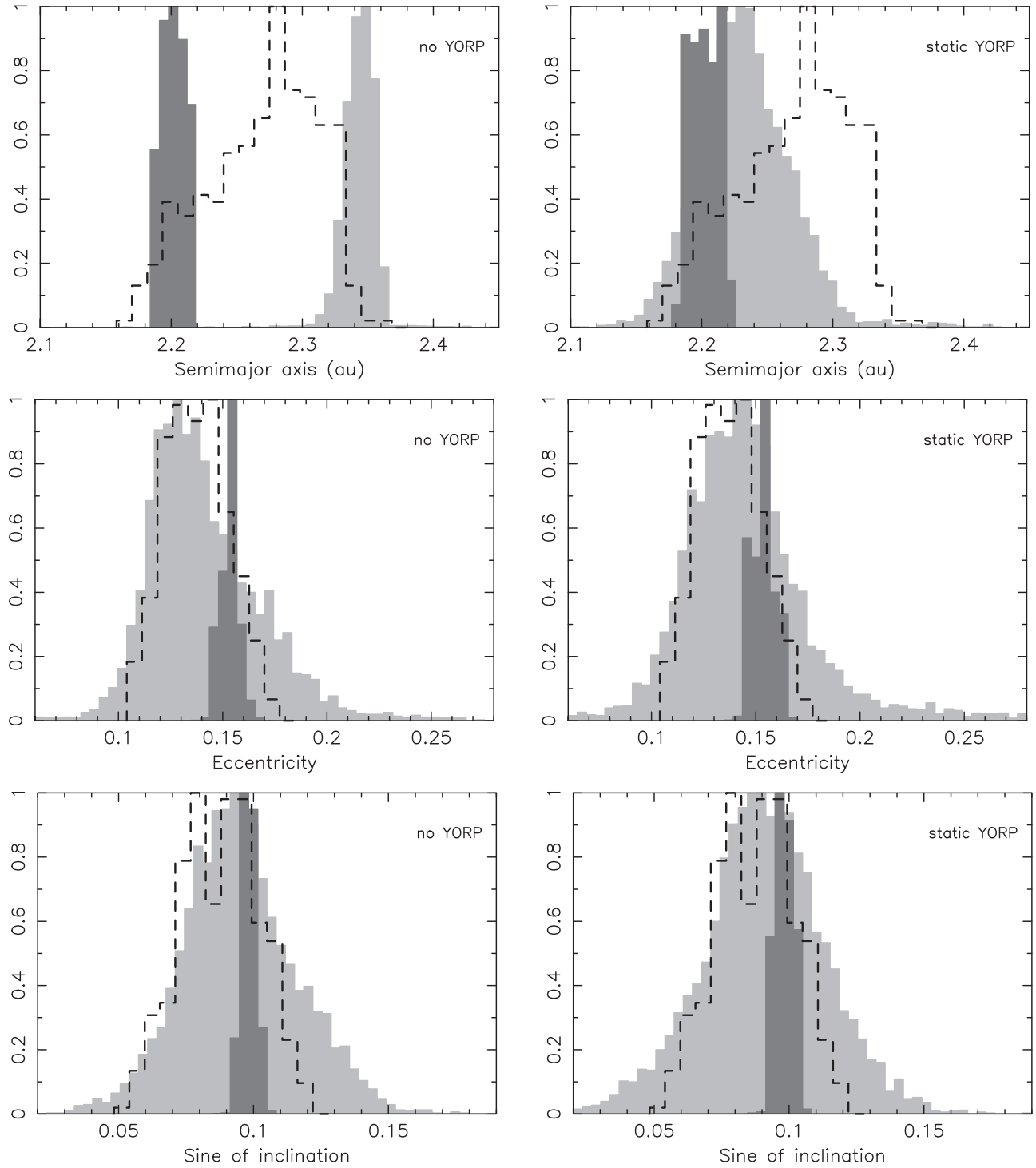

Figure 5. Distribution of $D = 3$ km size Flora-family fragments in proper semimajor axis (top), proper eccentricity (middle), and proper sine of inclination (bottom). The observed family data are shown by the dashed histogram. The synthetic family is represented by the filled histograms: (1) dark gray showing initial distribution, and (2) light gray showing distribution of asteroids remaining in the family zone at 1 Gyr. The left series of panels for the simulation are those where only the Yarkovsky effect was taken into account, with the obliquities set either to 0° or 180° (which maximizes the drift rate inward toward or outward away from the Sun). The right series of panels are those simulations where both Yarkovsky and static YORP effects were included. Initially, Flora fragments were launched isotropically away from the parent body with ejection velocities of 100 m s^{-1}.

Our model distributions of proper eccentricities and inclinations match the observed ones more closely than those for semimajor axes (see middle and bottom left panels in Figure 5). At 1 Gyr, the initially narrow distributions have appreciably broadened, with the tail values exceeding the distribution of the observed family. This matches the results discussed in Nesvorný et al. (2002b), who recognized the dispersive role of the weak mean-motion resonances, and the expected effects of the z_2 secular resonance.

Overall, it only takes about 0.5–0.6 Gyr to reach the full width of the observed Flora distribution in proper eccentricity and inclination space. After this elapsed time, the half-width of

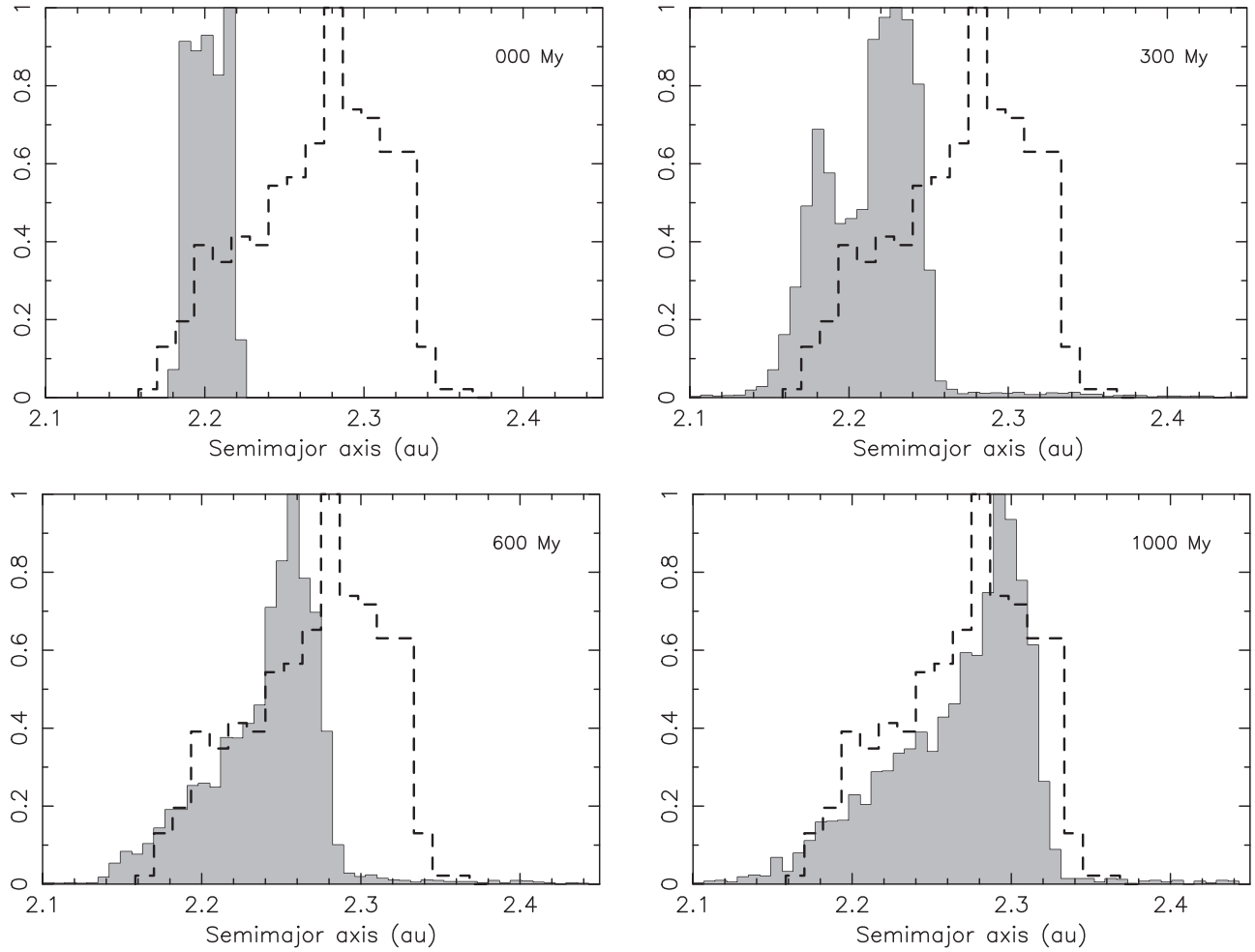

Figure 6. Proper semimajor axis distribution of $D = 3$ km Flora family fragments. The observed family data are shown by the dashed histogram. Results from our simulation of a synthetic family at four different evolution times, 0, 300, 600 and 1000 My, are shown with gray histograms. Initially, Flora fragments were launched isotropically away from the parent body with ejection velocities of 100 m s^{-1} (top and left). The Yarkovsky effect causes different fragments to drift to larger and smaller values of the semimajor axis, depending in their obliquity values. We used the stochastic YORP model with the $\mathcal{R} = 0.3$ parameter.

the distributions evolve more slowly but the tails keep spreading. At this point, however, the real Flora family members would likely disperse into the inner main belt far enough that they would be difficult to identify as family members using hierarchical clustering methods. As a consequence, the mismatch between model and data may not actually be a problem. This model predicts that Flora should have a halo structure, though one that can only be recognized if the family members stand out from the background population in some way (e.g., colors, spectra, albedo; see Brož & Morbidelli 2013, a nice example of this phenomenon is found for the Eos family). At the time of this writing, no halo has been identified amid the Flora background (though see comments in Section 6.4 of Nesvorný et al. 2015).

In our next set of idealized simulations, shown in the right panels in Figure 5, we include the Yarkovsky accelerations, the rotation state evolution model, and the static variant of the YORP effect. Here we see the opposite problem with the semimajor axis distribution than the one described above. The final semimajor axis distribution at 1 Gyr of the synthetic family has been broadened, but its mean value is only 2.24 au. This means it is incapable of matching the right ear of the observed Flora family, which peaks near 2.28 au.

Clearly, the static YORP effect makes the nominal YORP cycles too short, such that the spin axes of the asteroids reorient themselves too frequently. This implies that the Yarkovsky effect makes the bodies undergo a random walk in semimajor axes rather than steadily increasing or decreasing. Indeed, as mentioned above, the nominal $T_{\rm YORP}$ value for $D = 3$ km bodies is only $\simeq$25–50 Myr. Upon close inspection, we found that the longest steady trend in semimajor axis evolution only lasts several tens of megayears before it is taken over by the random-walk phase.

Note that while the semimajor axis distribution indicates this simulation is a failure, the proper eccentricity and sine of inclination distributions are still a good match to those of the observed Flora family for evolution times $\geqslant$0.5 Gyr. As before, the reason is that a multitude of weak mean-motion resonances between 2.2 and 2.25 au produce the needed dispersive effect on the family members.

The simulations described above used the case 1 initial orbital conditions for Flora family members (i.e., starting at a large value of the osculating eccentricity and small value of the osculating inclination; Figure 2). Our simulations for the case 2 initial orbital conditions did not show any noticeable differences. The reason is that the ejection speed of 100 m s^{-1} is too small to directly inject Flora fragments into

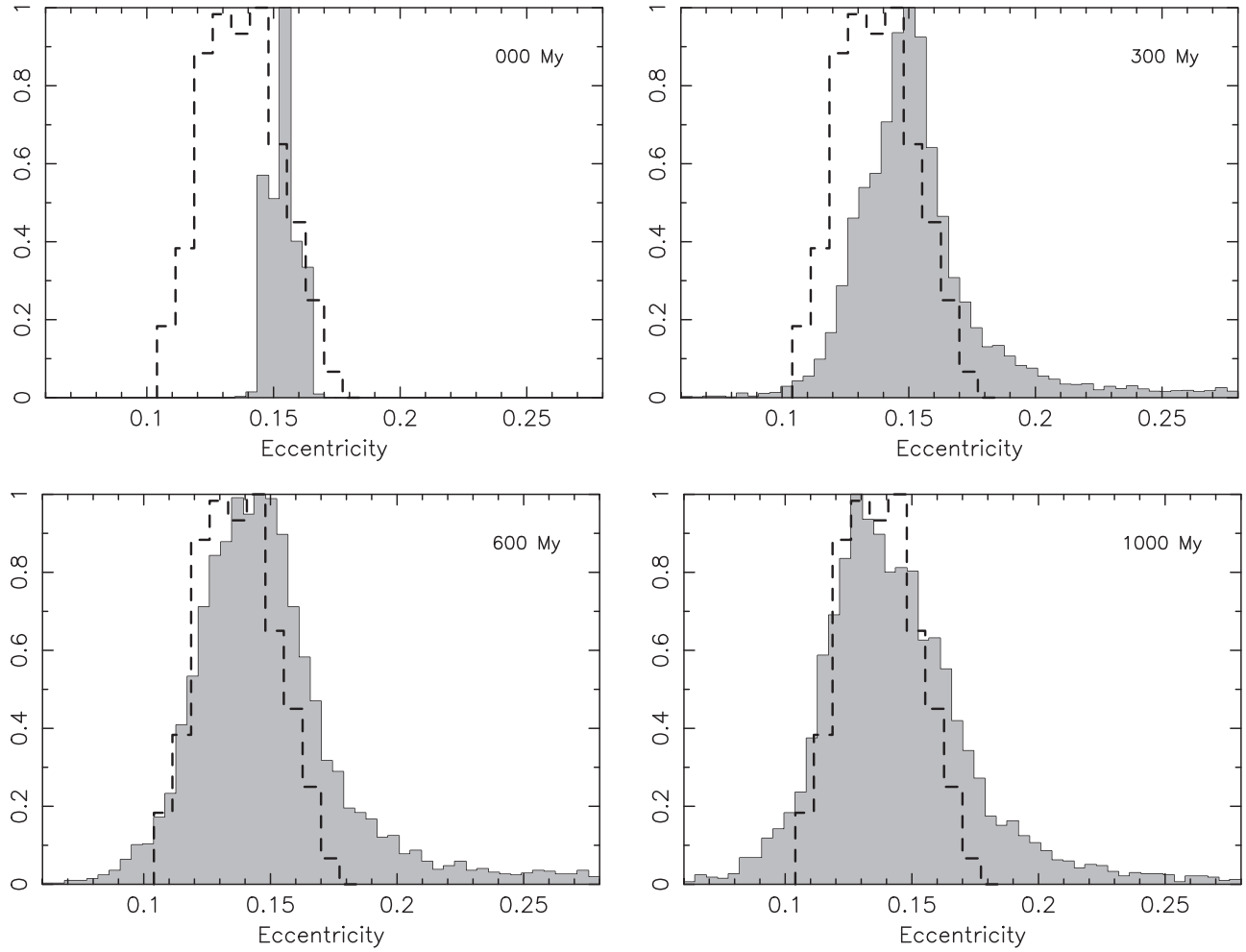

Figure 7. Comparison between the model and observed proper eccentricity distributions for the Flora family. See Figure 6 for additional details. The narrow and offset initial distribution (top and left) gradually becomes spread in time as the family members are initially placed in or are Yarkovsky-transported into weak mean-motion resonances with Mars and Jupiter. The full half-width of the observed family distribution is reached in ≃0.5 Gyr. At 1 Gyr, the tails or wings of the distribution continue to slowly spread, allowing small asteroids to diffuse from the identifiable family into a large halo zone surrounding the family.

the ν_6 resonance or the Mars-crossing zone (compare with Nesvorný et al. 2007). The similarity between case 1 and 2 results means that we will only discuss the case 1 simulation below.

The take away message from these simulations is that the optimum model needed to provide results that are somewhere between the no-YORP and the static YORP cases. Extending the characteristic timescale $T_{\rm YORP}$ would help the family members drift farther and reach the zone of the observed right ear of the Flora family. In this respect, one must consider that YORP effect theory has been undergoing rapid advances in the past several years (see Vokrouhlický et al. 2015, and references therein), with new results indicating it is a more complex phenomenon than envisaged by the earliest models (e.g., Rubincam 2000 or Čapek & Vokrouhlický 2004). In the following simulations, we examine how the stochastic YORP model deals with this problem. The reader should be aware, though, that our approximations may hide complexities that eventually need to be modeled with more accuracy.

4.2. Production Simulations

In this section, we discuss results from our runs where we included the stochastic YORP effect. As before, we use case 1 initial conditions with an initial ejection field of 100 m s^{-1} and conduct simulations for family members that are $D = 1$ km and $D = 3$ km. As explained in Section 3.2, the stochastic YORP model is in fact a one-parametric set of models with an empirical value of $\mathcal{R}$, the ratio between the timescale on which the surface properties are reset and the (static) YORP timescale $T_{\rm YORP}$. We ran simulations for $\mathcal{R} = 0.1$, 0.3, 1, and 3 to test the dependence of the results on this parameter.

We found that the simulation with $\mathcal{R} = 0.1$ suffers similar problems to the above discussed simulation where only the Yarkovsky effect was included, while simulations with $\mathcal{R} = 1$ and $\mathcal{R} = 3$ experienced similar problems to the above discussed simulation where only the static YORP effect was included. Out of our starting choices, $\mathcal{R} = 0.3$ provided the best results. We suspect that $\mathcal{R}$-values near 0.3 would also work but we did not characterize this range for computational expediency.

Figure 6 shows several snapshots of how the semimajor axis distribution of the synthetic Flora family members changes with time for $D = 3$ km. At ≃1 Gyr, the modeled distribution matches the observed one reasonably well, albeit with some small differences. We believe these small mismatches could be accommodated by choosing slightly different initial ejection speeds for our Flora fragments and/or a slightly different value

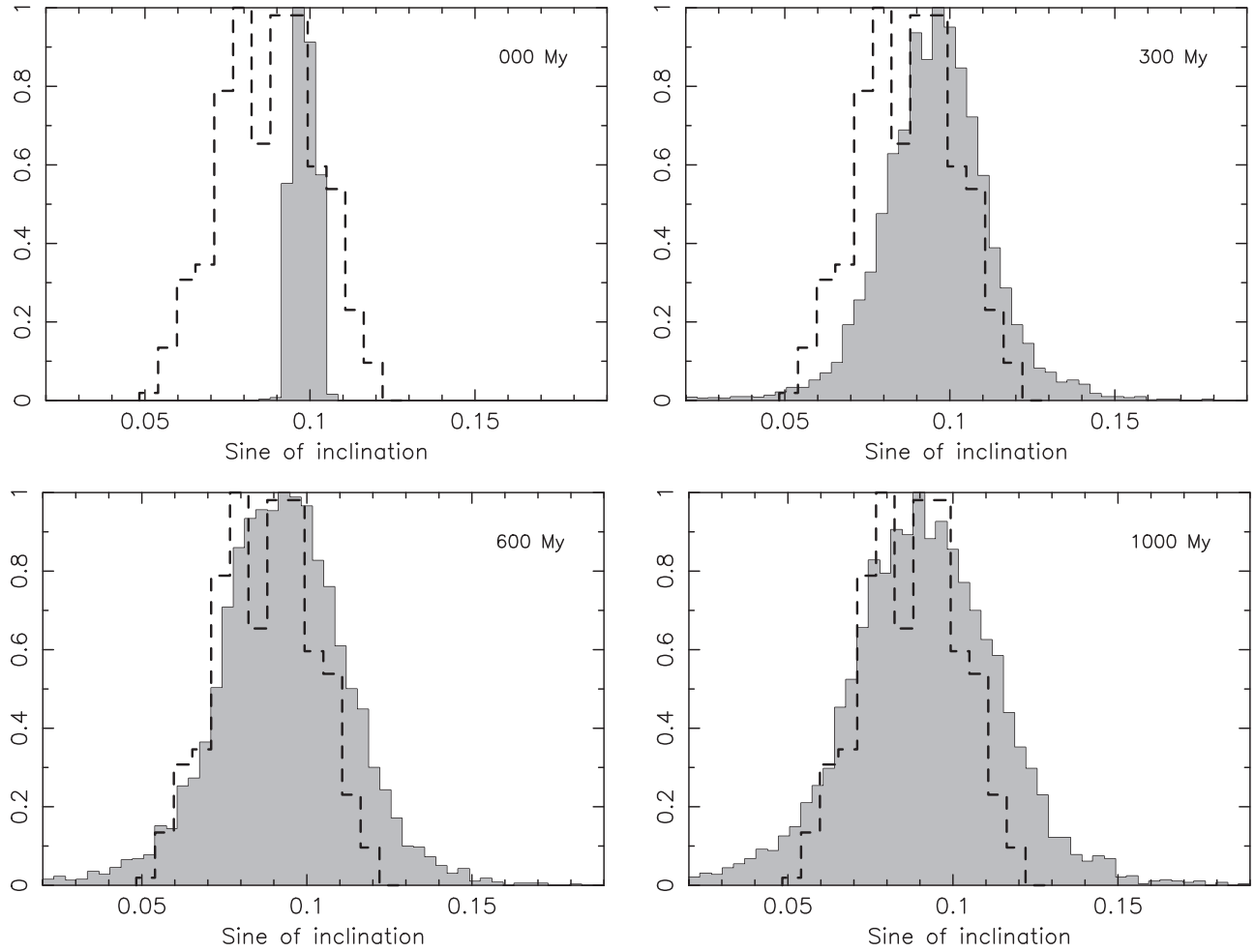

Figure 8. Comparison between the model and observed proper sine of inclination distributions for the Flora family. See Figure 6 for additional details. Weak mean-motion resonances produce the same diffusive dynamical effects as in the eccentricity case.

of $\mathcal{R}$. Testing all such values, however, is computationally expensive. For that reason, we cannot determine an exact age or age limits for the Flora family from our work. Nevertheless, a value of $\geqslant$1 Gyr seems plausible for our preferred choice of parameters.

Figures 7 and 8 show corresponding snapshots for the eccentricity and inclination evolution of the synthetic Flora family in our simulation. Except for tails at small and large values of the respective orbital element, which are perhaps of no significant concern because they describe the yet-to-be convincingly identified Flora family halo, the match to observations is reasonably good for $\geqslant$0.5 Gyr. Thus, the age of the Flora family is set mainly by our ability to reproduce the observed semimajor axis distribution.

Figure 9 shows the evolutionary tracks of 200 randomly chosen synthetic Flora family members from our simulation in mean orbital element space (approximating the proper elements; showing all 10 000 asteroids in our run would saturate the figure). Here we see the main evolutionary trends in action: (1) the Yarkovsky effect makes the bodies in the semimajor axis move away from their formation location near $\simeq$2.2 au (location of (8) Flora; see Figure 4), and (2) interaction with mean-motion resonances that help stretch the eccentricity and inclination distributions of the bodies. The latter diffuse into a broad Flora family halo or escape from the main asteroid belt by reaching a Mars-crossing orbit.

The most powerful escape route is the ν_6 resonance located near 2.15 au for asteroids with the mean inclination of Flora members. Orbital evolution of some family members is also directed along a diagonal pathway leading to higher eccentricities and inclinations as the semimajor axis increases. Those became trapped in the nonlinear secular resonance z_2 (see, e.g., Milani & Knežević 1992, 1994). Some of the principal weak mean-motion resonances were identified using data in Figures 1–4 of Morbidelli & Nesvorný (1999). For reference, we use nomenclature that follows these two examples: M7/12 for the exterior 7:12 mean-motion resonance with Mars and J7/2 for the 7:2 interior mean-motion resonance with Jupiter. Figure 10, now for $D = 1$ km asteroids, lets us appreciate how stronger Yarkovsky drift rates affect semimajor axis evolution for smaller objects. The main dispersive effect due to weak mean-motion resonances is about the same as for the $D = 3$ km objects above.

The left panel of Figure 11 shows how our synthetic Flora family became dynamically depleted in $D = 1$ km and $D = 3$ km asteroids over time. For instance, given a $\simeq$1 Gyr age of the family, we note that the family was dynamically depleted in $D = 1$ km and $D = 3$ km asteroids to $\simeq$33% and $\simeq$40% of the initial population, respectively. In order to make use of these data to calibrate the family (i.e., to know its initial population at those sizes), however, we need to account for one more effect. The billion year old Flora family is ancient enough

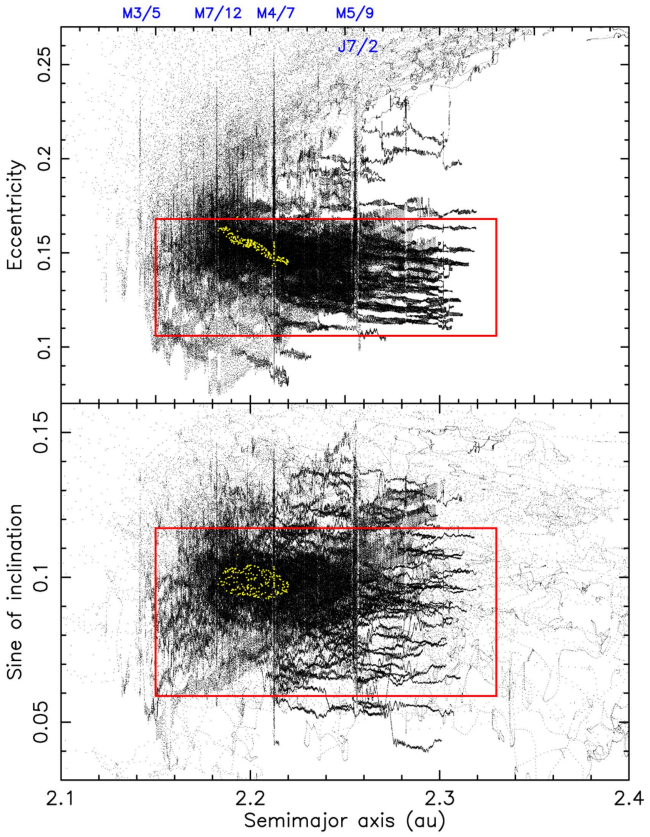

Figure 9. Evolutionary tracks of 200 $D = 3$ km size asteroids in our simulation with stochastic YORP included and $\mathcal{R} = 0.3$. Mean orbital elements were computed over a sliding 5 Myr wide window. They are used as a proxy of the proper orbital elements: semimajor axis at the abscissa, eccentricity, and sine of inclination at the ordinate (top and bottom). The figure shows the full extent of our 1 Gyr long integration; many family members escape at earlier epochs via the ν_6 resonance or through weak mean-motion resonances (blue labels at the top). The red rectangle shows the nominal extension of the $D = 3$ km Flora members: mean value plus and minus 2σ of the distributions in the respective proper elements (Section 2). The orbital position of (8) Flora is $a_8 = 2.2014$ au, $e_8 = 0.1544$, and $\sin i_8 = 0.0998$. The yellow symbols are the mean elements computed from the first 5 Myr of the initegration (a.k.a., the initial data).

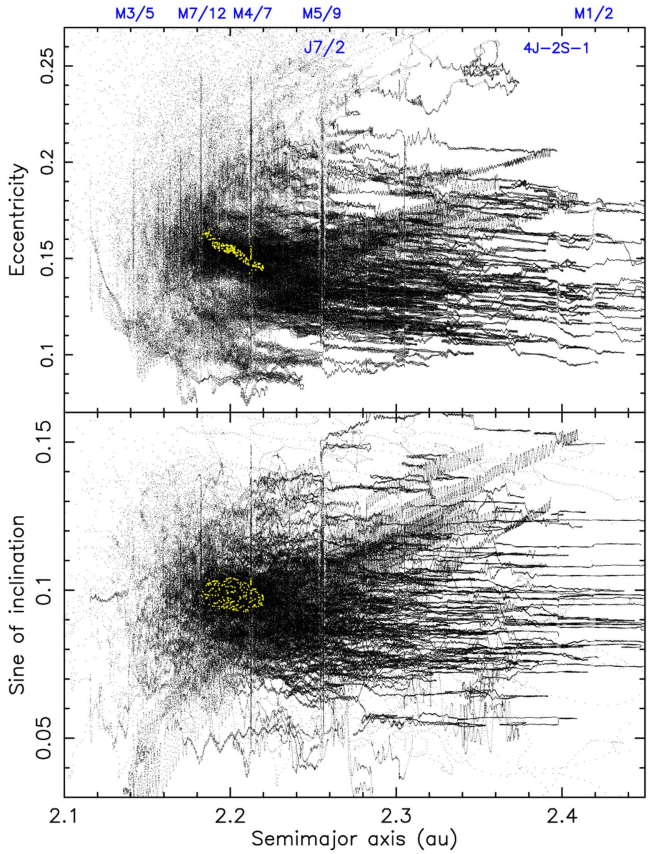

Figure 10. Same as in Figure 9 but now for $D = 1$ km size asteroids.

to have experienced substantial collisional evolution among family members, according to numerical simulations (e.g., Bottke et al. 2005, 2015a). Impacts act both as a source and sink for family members; smaller bodies are disrupted more readily than larger ones, but the occasional breakup of a large family member may replenish, at least in part, the number of smaller family members. Modeling results also show that collisions grind a family's size frequency distribution (SFD) into a shape that eventually begins to mimic that of the main-belt SFD. Given that most asteroids escape the main belt via slow but steady Yarkovsky thermal forces, which deliver them to powerful resonances that can push them onto planet-crossing orbits, collisional evolution explains why the shape of the NEO SFD, as well as the crater SFDs found on Mercury, Venus, Moon, and Mars over the last several billions of years, all resemble the shape of the main belt's SFD (e.g., Bottke et al. 2015a).

To estimate how collisional evolution has effected the Flora family, we turn to the family evolution runs described in Bottke et al. (2005). The existing Flora family for $D \geqslant 1$ to 3 km asteroids, both as described in this paper and in Masiero et al. (2013), and also used in our Section 2, is reasonably similar to the Bottke et al. (2005) model run where they investigated the evolution of a synthetic-family SFD produced by the breakup of a $D \simeq 100$ km asteroid. Computation details are provided in that paper. We find that over 1 Gyr of collisional evolution, the cumulative number of $D \geqslant 1$ to 3 km asteroids, $N(1)$ and $N(3)$ decreases by factors of $\simeq$3.3 and $\simeq$1.5, respectively. For 1.5 Gyr of collisional evolution, the decrease is by factors of $\simeq$5 and $\simeq$1.7, respectively. Accordingly, we must use these values in conjunction with the dynamical decay factors and the present-day number of $N(1)$ and $N(3)$ to estimate the initial size of the Flora family. Only then can we accurately estimate how the impact flux striking Venus, Earth, the Moon, and Mars from Flora changed over time.

Therefore, combining the results from both panels in Figure 11, and using population counts of today-observed Flora family in Section 2, we estimate the initial family counts to $N(1) \simeq 116\,000$–$160\,000$ and $N(3) \simeq 2\,600$–$3\,350$. Given the uncertainties of collisional and dynamical modeling, we only use one realization of family evolution, though we would argue that our values are reasonable given current knowledge.

Contribution to the NEA population. Now that we have dynamically reproduced the orbital properties of the observed Flora family, and we have an estimate for its age, we can consider how its members potentially affected the terrestrial planets. We are interested in the fate of the $\simeq$(60–70)% of the $D = 1$ km and $D = 3$ km family members that escaped onto planet-crossing orbits. In particular, we want to know to what extent this population contributed to the ancient NEA population.

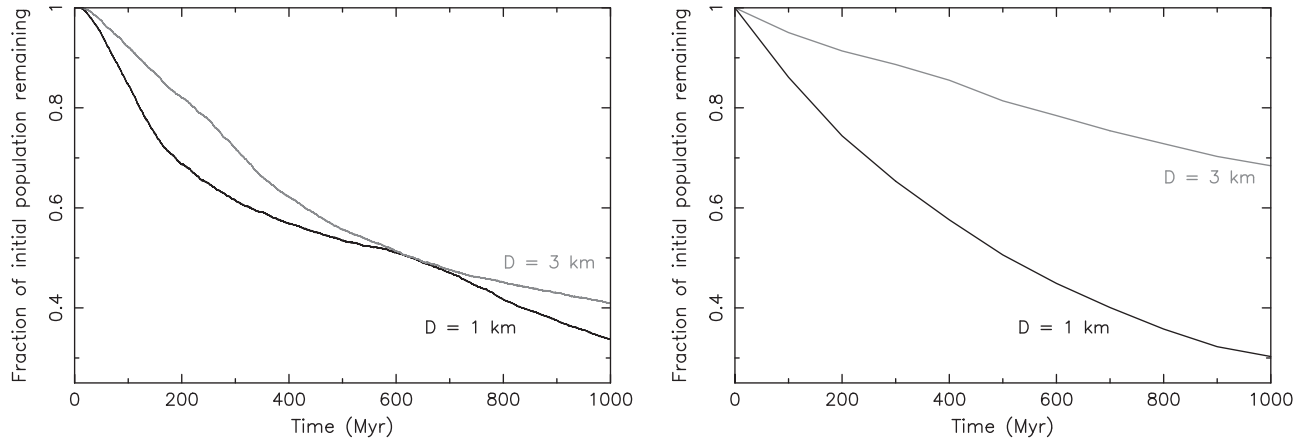

Figure 11. Left panel: fraction of the initial population of 10 000 particles of our synthetic-family evolution remaining in the nominal zone of the Flora family defined by the mean value plus and minus 2σ dispersion in the three proper orbital elements and for the respective size of bodies (e.g., for $D = 3$ km objects, this is shown by the red rectangle in Figure 9). The black curve for $D = 1$ km asteroids, the gray curve for $D = 3$ km asteroids. These data define dynamical decay of the Flora family population. Right panel: fraction of initial population in the Flora family that survives collisional evolution (mostly driven by impacts due to the background-asteroid population). The black curve for $D \geqslant 1$ km asteroids, the gray curve for $D \geqslant 3$ km asteroids. These data define the collisional decay of the Flora family population.

Nearly all of the Flora family members that reached planet-crossing orbits hundreds of megayears ago or more have been eliminated from the inner solar system. This is because the characteristic lifetime of objects on NEA orbits is $\simeq$6 Myr (e.g., Bottke et al. 2002a), a timescale much shorter than the estimated age of the family. This raises the interesting question of how much the Flora family is contributing to today's NEA population.

In our simulations, we determined the orbit fate of all of the family members (see Section 3). Typically, a family member escaping the main belt spent some time in the NEA population prior to being eliminated from the simulation. We recorded this phase and plotted a summary of the information in Figure 12. Here we used our best-fit simulation above with stochastic YORP set to $\mathcal{R} = 0.3$. At each output, every 5 kyr, we recorded active orbits in our simulation with perihelia $\leqslant$1.3 au (i.e., where they reach the NEA population). We also smoothed the orbital evolution signal using 5 Myr averages computed using a sliding window; this was done because the perihelia of the escaped family members often oscillate near the 1.3 au value. In our runs, we also determined the fraction of the total that reached individual sub-populations of NEAs, such as Amor, Apollo, and Aten orbits, according to the standard definitions (e.g., Bottke et al. 2002a). These are shown in different colors on Figure 12.

As expected, there is a strong time dependence in Flora's contribution to the NEA population, especially for smaller $D = 1$ km asteroids. For example, the population of $D = 1$ km NEAs peaks between 100 and 200 Myr after the family-forming event. This could be described as a wave of fragments that invade the planet-crossing zone in the aftermath of Flora family's formation. After this phase is complete, the already depleted population of $D = 1$ km family members enters a phase where YORP cycles allow some of the asteroids moving away from the ν_6 resonance to reverse their direction, and vice versa. The net effect is that the flux into the escape hatches decreases.

The contribution of $D = 3$ km asteroids to the NEA population also shows important time dependence. We see a broad increase taking place between $\simeq$100 and 450 Myr after the family-forming event in Figure 12, with a broad peak near 300 Myr. This slow increase, a fairly long plateau feature, and a slow decrease is consistent with the fact that $D = 3$ km asteroids take longer to escape the main belt than smaller bodies.

At 1 Gyr, the contribution to the NEA population is nearly an order of magnitude smaller than during its peak at $\simeq$150 Myr for $D = 1$ km asteroids. The net decrease is smaller for $D = 3$ km family members (right panel on Figure 12); a factor of four or so from the "plateau." Intriguingly, the relative contributions to the Amor, Apollo, and Aten sub-populations are about the same as those observed and predicted by NEA population models (e.g., Bottke et al. 2002a; Granvik et al. 2016). For example, the contributions to the Amor and Apollo populations are about the same, with the Apollo population occasionally being larger, while the Aten population is generally about an order of magnitude smaller than the other two.

Given our estimate of the initial populations of $D \geqslant 1$ km and $D \geqslant 3$ km fragments in the Flora family, we may now turn our data in Figure 12 into absolute numbers. Note that this procedure also requires us to take into account the collisional evolution of the family; we do it using the data shown in the right panel of Figure 11. Our simulation then predicts that in the peak of the Flora family's contribution to the NEA population, it contributed approximately 815–1 120 $D \geqslant 1$ km asteroids, and 14–18 $D \geqslant 3$ km asteroids to the NEA population. This is comparable, or slightly larger than, the current number of NEAs for $D \geqslant 1$ km bodies. Consider that Harris & D'Abramo (2015) derive that there are 990 ± 20 such bodies in the NEA population today (for a comparison, Granvik et al. 2016 give $1\,008 \pm 45$ from a different model). In contrast, our runs suggest that the current Flora family input to the NEA population has dropped to 35–50 $D \geqslant 1$ km asteroids and about 2 $D \geqslant 3$ km asteroids. This result will be further discussed in Section 5.

In order to determine how our results depend on the choice of the $\mathcal{R}$ parameter of the stochastic YORP model, we set $\mathcal{R}$ to 0.1, 0.3, 1, and 3 and computed the production rate of $D = 1$ km NEAs in Figure 13. The reader should keep in mind that cases $\mathcal{R} = 1$ and $\mathcal{R} = 3$ do not allow our model family to reproduce the semimajor axis distribution of the observed Flora family. The $\mathcal{R} = 0.1$ case is better and modestly close to making a match for the $D = 3$ km family members, though it

would probably require the family to be older than 1 Gyr to reach a best fit. With these caveats in mind, we note that the Flora contribution to the NEA population depends on the choice of $\mathcal{R}$ as far as the peak-contribution is concerned, but less so in the later phase when the flux drops. The $\mathcal{R} = 0.1$ may indicate even larger peak-contribution, up to $\simeq$1.25% of the initial population in the family. This is in agreement with the fact that this model is closer to the maximum drift case when only the Yarkovsky effect was included in the simulation. The opposite is true for the $\mathcal{R} = 1$ and $\mathcal{R} = 3$ cases.

Planet impacts. We also used results from our simulations to characterize the impact flux of Flora fragments on Venus, Earth, and Mars. The Moon's impact flux can be obtained by using the Earth's flux and dividing by a factor of $\simeq$20 (e.g., Ito & Malhotra 2010). This was done using two methods. In the first method, as discussed in Section 3, one of the endstates of Flora family members in our simulation was to impact a planet or the Sun. We thus collected all directly recorded planetary impacts in our simulations. The strength of method 1 is that it is exact, but its downside is that it could suffer from small number statistics. In the second method, family members reaching planet-crossing orbits had their impact probabilities for Venus, Earth, and Mars evaluated at every output timestep using the Öpik method (see Greenberg 1982; Bottke & Greenberg 1993; Bottke et al. 1994). The strength of method 2 is that it is based on a much larger sample of orbits than just direct impacts. The downside is that it is fairly approximate because it implicitly assumes equal contributions from all asteroid-planet configurations over the orbit angles (i.e., longitudes of node and pericenter are assumed to uniformly span the interval of 0° to 360°). Recent work has shown that this assumption breaks down for many known NEAs (e.g., JeongAhn & Malhotra 2014, 2015).

Figure 14 shows a cumulative number of planetary impacts for 1 Gyr after the Flora family formed for our nominal run with stochastic YORP and $\mathcal{R} = 0.3$. Interestingly, the cumulative values of impacts at the end of the simulation are about the same for $D = 1$ km and $D = 3$ km family members, if expressed in terms of their initial population in the Flora family. Their time profile, however, is different; $D = 1$ km impactors hit mostly in the early phase of simulation (compare with their peak contribution to the NEA population in Figure 12), while the $D = 3$ km impact profile is more uniformly spread over the entire time interval of the simulation.

The distribution of directly recorded impacts and those estimated from our impact probability calculations are reasonably similar except for two effects: (1) the latter seems to overestimate the number of impacts for Mars and $D = 3$ km objects (top and right), and (2) in both cases, we recorded more direct impacts on Venus than expected from the Öpik method. A plausible reason for (1) may have to do with a fraction of Flora members leaking out from the family zone via exterior mean-motion resonances with Mars (see, e.g., Figure 9). If bodies are captured in these resonances, they are protected for some time from Mars impacts, and the Öpik method does not account for this. The reason for (2) is unknown to us.

We found that 0.9%–1.1% of Flora fragments impacted Earth and Venus after 1 Gyr of family evolution. Venus was favored as an impact target over Earth by a factor of $\simeq$1.2 in both the $D = 1$ and 3 km simulations, while the fraction hitting Mars tended to be half as big as that hitting Earth. Overall, the results also indicate that 1.7%–2.0% of those bodies that escaped from the main belt hit Earth or Venus. This fraction compares favorably with other calculations for bodies reaching the ν_6 resonance (e.g., Morbidelli & Gladman 1998; Zappalà et al. 1998; Bottke et al. 2006a). This fraction is high compared with other major escape routes out of the main asteroid belt; for example, Bottke et al. (2006a) found that 0.3%, 0.03%, and 0.01% of test body population started in the Jupiter's J3/1, J5/2, and J2/1 mean-motion resonances struck Earth, respectively. Accordingly, it is expected that the Flora family was likely a prominent contributor not only to the NEA population but also to terrestrial planet impactors.

Having estimated the initial population of Flora fragments above, we now use our dynamical model predictions from Figure 14 and our collisional evolution estimates from Figure 11 to make more quantitative estimates of the impact flux on different worlds. Putting these values together, we estimate that there have been 690–950 $D \geqslant 1$ km and 19–24 $D \geqslant 3$ km impacts of Earth from the Flora family over the last 1 Gyr, provided the family formed 1 Gyr ago. Slightly larger values are expected for Venus, and about half as many are expected to hit Mars. Assuming the ratio of impacts on the Earth and Moon is $\simeq$20 (e.g., Ito & Malhotra 2010), we estimate that the Moon was struck about 34–47 times and $\simeq$1 time by $D \geqslant 1$ km and $D \geqslant 3$ km Flora asteroids, respectively, over the past 1 Gyr. The largest Flora impactor size that hit the Earth over a 1 Gyr interval from the Flora family was $\simeq$6–6.5 km.

4.3. Additional Simulations

In Sections 4.1 and 4.2, we used 100 m s^{-1} as the initial characteristic velocity with which fragments were ejected from the parent body. We consider this value to be well justified because it is close to the estimated escape velocity. However, for the sake of comparison, we also ran a limited set of simulations with a larger $v_{\rm ej}$ value, namely 300 m s^{-1}. While this value is likely an exaggeration, our goal here is to probe sensitivity of the results on $v_{\rm ej}$. We used case 1 initial configuration of (8) Flora (Figure 2), stochastic YORP model with $\mathcal{R} = 0.3$ parameter, and we ran simulations for $D = 1$ km and $D = 3$ km fragments.

Figure 15 shows semimajor axis distribution of the synthetic fragment population of $D = 3$ km asteroids compared to the currently observed population for four epochs of our simulation. The initial distribution (top and left) is three times wider than in Figure 6, a direct consequence of the chosen velocities. This has two effects. First, some fragments have been initially ejected into, or very close to, the ν_6 resonance and these are swiftly evolving to the terrestrial planet orbital region. Second, some fragments have been ejected to quite larger initial semimajor axis values, up to $\simeq$2.26 au, than in the previous case with $v_{\rm ej} = 100$ m s^{-1}. These fragments, if they have suitable orientations of their spin axes for a sufficiently long time, may have a chance to reach the family extreme values of $\simeq$2.35 au in a shorter time then seen in the production simulation in Section 4.2. Indeed, the bottom right panel shows the semimajor axis distribution of the synthetic family at 850 Myr matching the observed family reasonably well. The fit is even somewhat better than in the last panel of Figure 6, because the modeled distribution evolves to be wide enough to compare well with the observed data. While being an advantage for the semimajor axis, this trace of the initially wider distribution becomes a caveat in the distributions of the proper eccentricity and sine of the inclination shown in Figure 16

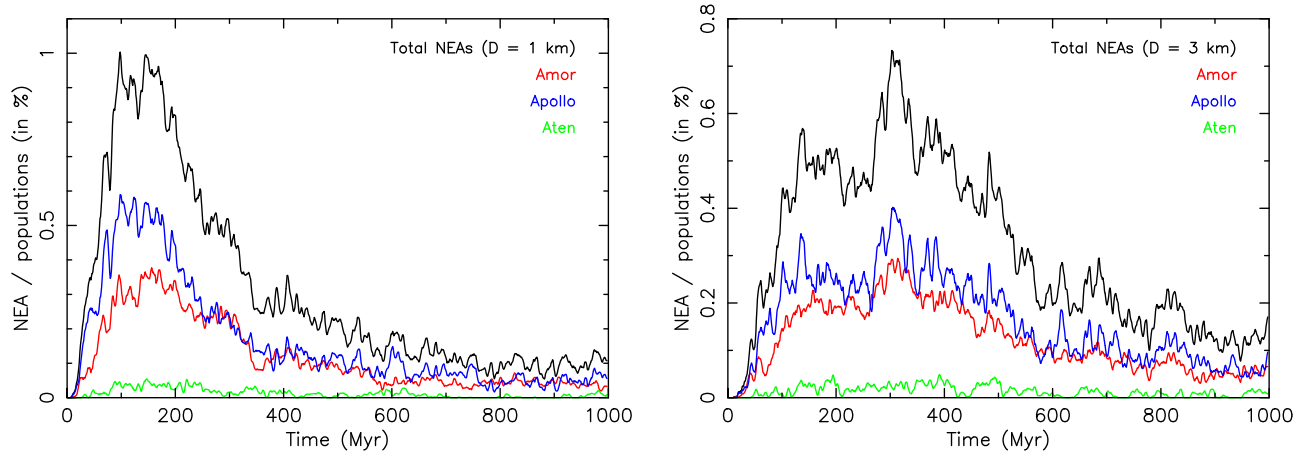

Figure 12. Number of Flora family members asteroids pushed onto NEA orbits in our simulation with stochastic YORP included and $\mathcal{R} = 0.3$. No collisional evolution has been included to make these figures. The signal has been smoothed by averaging over a 5 Myr wide sliding window to remove high-frequency jitter from orbits whose perihelia oscillate near perihelion $q = 1.3$ au. Left panel: $D = 1$ km asteroids. Right panel: $D = 3$ km asteroids. The total NEA contribution is shown by the black curve, while contributions to Amor, Apollo, and Aten sub-populations are shown by color curves. Time since the family formation event took place is on the abscissa. The population abundance at the ordinate is expressed as a fraction of the initial population of objects in the Flora family zone (this was 10 000 in our synthetic family).

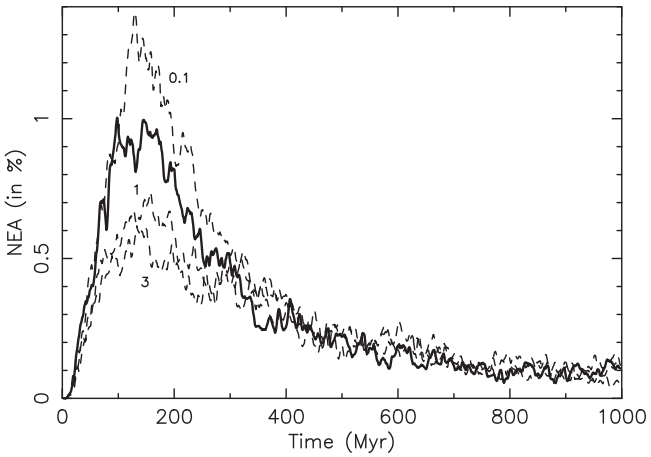

Figure 13. Contribution of the Flora family to the NEA population of $D = 1$ km asteroids, provided as a fraction of the initial number of Flora asteroids of this size. No collisional evolution was included. The total number of NEAs is shown as a solid line and is the same as the solid line in Figure 12. Here the stochastic YORP parameter was set to $\mathcal{R} = 0.3$. The dashed lines provide results for different values of $\mathcal{R}$: 0.1, 1, and 3.

(again at 850 Myr). Note that the synthetic family has now broader wings toward smaller and larger values than observed in the nominal family (obviously, part of this mismatch may be due to an unidentified halo of the Flora family at larger relative distance-cutoff in the space of proper orbital elements). Despite some of the fragments initially being launched into the ν_6 resonance, the fraction of Flora members that survived in the main belt is only slightly smaller than that shown in Figure 11.

Figure 17 shows a fractional contribution of the synthetic-family ejecta to the NEA population and its parts as a function of time since the formation of the family. Note that the current epoch in these figures should be at $\simeq$850 Myr. If compared to results in Figure 12 from our production simulations, we see some changes. The most obvious feature happens during the first $\simeq$200 Myr after the family formed, namely a stronger peak in Flora fragments among NEAs (both for $D = 1$ km and $D = 3$ km asteroids). This is due to the initial injection of fragments into, or very near, the ν_6 resonance. In quantitative terms, at the peak of the initial surge, there might have been as many as 1 170–1 680 $D \geqslant 1$ km and 28–36 $D \geqslant 3$ km Flora fragments in the NEA population. These numbers are quite high compared to currently observed NEAs of these sizes (e.g., Harris & D'Abramo 2015). However, when this initial wave ends, the long-term contribution is about the same as in our production runs. This is particularly true for the current epoch. In other words, even if we knew which large NEAs currently in the population are Flora fragments, their abundance would not teach us about the exact age of the family. The profile of the planetary impacts by Flora fragments is modified in the same way their influx into the NEA population has been changed. In particular, there are more early impacts during the first few hundreds of megayears. However, their total number accumulated over the age of the Flora family is about the same as that shown in Figure 14.

The takeaway message from this section is that there exists a correlation between the stated age of the Flora family and the characteristic initial dispersal velocity of the fragments with respect to the largest remnant (8) Flora. The smaller velocity and older age, on one hand, may be traded for larger velocity and younger age, on the other hand. Obviously, there are some limits in which this procedure could be pushed.

5. Discussion and Conclusions

5.1. Bombardment and Age Constraints on the Flora Family

Our numerical simulations indicate that the Flora family may have been a prodigious source of impactors for the terrestrial planets (i.e., the family once had numerous multi-kilometer and kilometer-sized fragments, many of them reached planet-crossing orbits, and a few percent of those hit the terrestrial planets). In addition, we find that the majority of these impacts occurred within 300–500 Myr of the family-forming event (Figure 14). Our work also suggests that family is at least 1 Gyr old. Taken together, we can begin to make comparisons between our model impact signatures and what is known about the nature of bombardment between 0.5 and 2.0 Ga from other data sets.

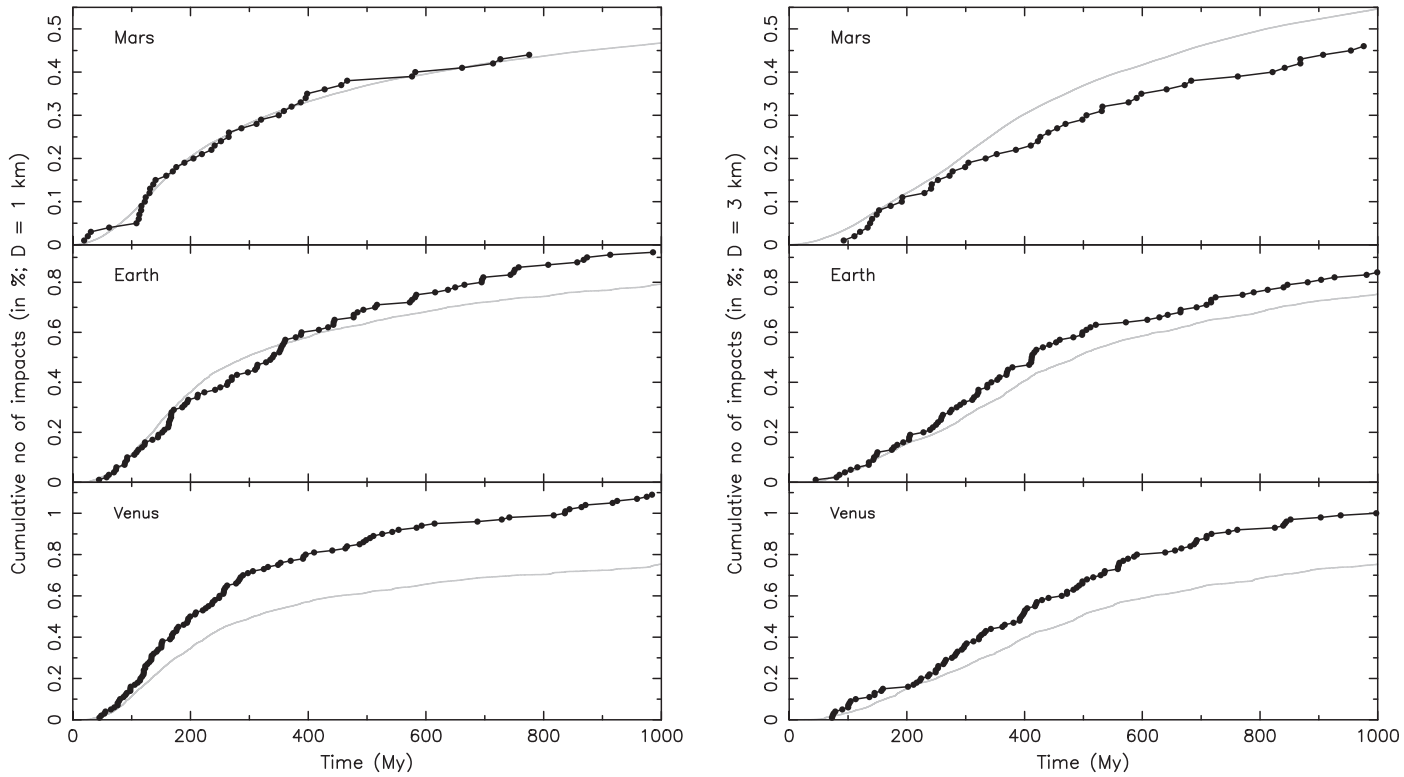

Figure 14. Cumulative number of impacts on different terrestrial worlds estimated from our synthetic Flora family simulations with stochastic YORP set to $\mathcal{R} = 0.3$. Black symbols record impacts in the simulation, while the gray curves provide values predicted by the Öpik impact probability theory. The left panels show results for $D = 1$ km asteroids striking Mars, Earth, and Venus, while the right panels show the same for $D = 3$ km asteroids. Time after the formation of the Flora family is given on the abscissa. The ordinate is the number of impacts as a fraction of the total initial number of Flora fragments of that diameter (though many family members never leave the main belt). No direct impacts on Mars were recorded in our simulation in the upper left panel ($D = 1$ km) past 800 Myr.

Before doing so, however, we caution the reader that very few hard constraints exist in this time interval. The Earth is nearly devoid of impact craters between 0.5 and 2.0 Ga (e.g., Spray 2017), Venus's surface is almost certainly too young to have received the brunt of Flora family impactors (e.g., McKinnon et al. 1997; Bottke et al. 2016), and lunar crater chronology, which is used to benchmark the crater chronologies of Mercury and Mars, is at best only modestly constrained between 0.5 and 2.0 Ga (e.g., Wilhelms 1987). Still, some useful information does exist, provided our interpretation of it has not been skewed by selection effects, etc. The following discussion is our attempt to piece together a story from the existing clues. Caveat emptor!

Lunar craters formed over the last billion years. We start our discussion with what is known about the lunar impact flux between 0.5 and 2.0 Ga. Using a new method for estimating the ages of lunar craters based on the thermophysical characteristics of impact ejecta (Ghent et al. 2014), Mazrouei et al. (2017) found the production rate of $D > 10$ km craters formed over the last 1 Gyr. They argue that the lunar impact flux increased by a factor of two to three over the past ∼0.2 to 0.3 Gyr. This reasonably matches predictions derived from the ages of impact spherules found in lunar regolith; they indicate that the impact flux was 3.7 ± 1.2 times higher over the last ∼0.4 Gyr (Culler et al. 2000). They also found that the production rate of $D > 10$ km craters was fairly constant and relatively low 0.4–1.0 Gyr ago. Thus, if Flora did form ≃1 Ga, and the impact profiles in Figure 14 are valid, one might expect to see a surge in the production rate of $D > 10$ km craters somewhere between, say, 0.7–1.0 Ga. The absence of such an increase suggests that (1) the Flora family was smaller than suspected or (2) the Flora family is older than 1 Ga. We favor the latter point for reasons described below.

Gaspra craters. As discussed above, crater spatial densities on (951) Gaspra, a Flora family member, are higher than that found on (4) Vesta's Rheasilvia basin, which appears to have formed ∼1 Ga (e.g., Marchi et al. 2014, 2015; Lindsay et al. 2015). The same crater production models used to date Rheasilvia's surface and ejecta blanket indicate Gaspra's surface, and perhaps the Flora family, is ∼1.5 Ga. This age is nearly 0.5 Gyr older than suggested by nominal results from our dynamical model, but it is not unreasonable provided we modify some of our starting conditions.

For example, according to Yarkovsky theory, the age of a family is directly proportional to the bulk density of its constituents (i.e., $T \propto \rho$), such that higher densities lead to older ages (e.g., Vokrouhlický et al. 2006a; Bottke et al. 2007). In our paper, we assumed our Flora family members had a bulk density of $\rho = 2\,\mathrm{g\,cm^{-3}}$, a value consistent with S-type asteroid Itokawa and other small S-type asteroids (e.g., Carry 2012). Estimates that include all S-type asteroid densities (including larger bodies), however, indicate that a preferable value may be $\rho = 2.70 \pm 0.54\,\mathrm{g\,cm^{-3}}$ (e.g., Scheeres et al. 2015). Accordingly, using this value, we should increase the age of the Flora family by $(2.7 \pm 0.54)/2 \times 1$ Gyr or 1.35 ± 0.3 Gyr. This value is a better match to Gaspra, and it suggests much of the so-called asteroid surge took place beyond the constraints provided by Mazrouei et al. (2017). This

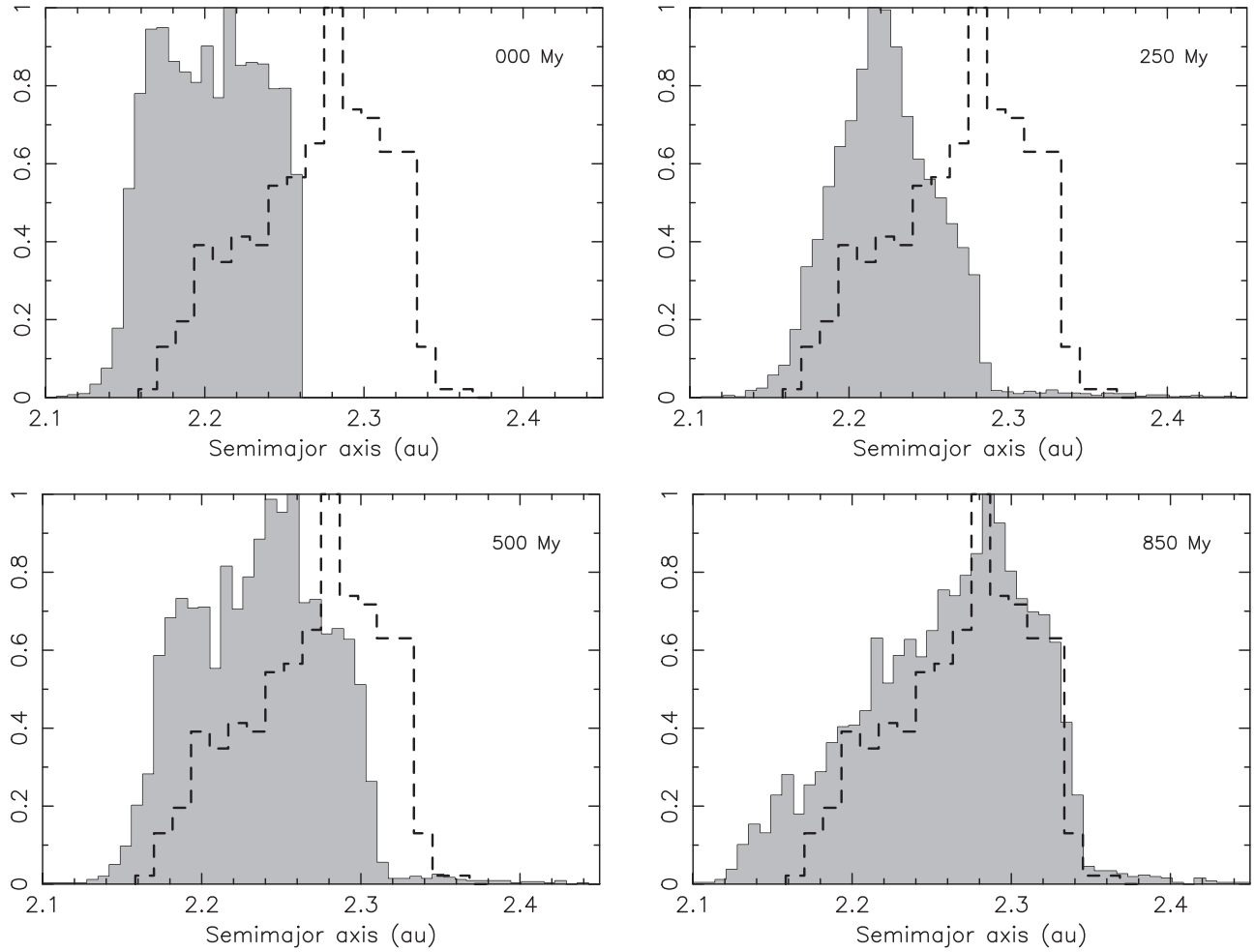

Figure 15. Proper semimajor axis distribution of $D = 3$ km Flora family fragments. The observed family data are shown by the dashed histogram. Results from our simulation of a synthetic family at four different evolution times, 0, 250, 500, and 850 My, are shown with gray histograms. Initially, Flora fragments were launched isotropically away from the parent body with ejection velocities of 300 m s^{-1} (top and left). The Yarkovsky effect causes different fragments to drift to larger and smaller values of the semimajor axis, depending in their obliquity values. We used the stochastic YORP model with the $\mathcal{R} = 0.3$ parameter.

older age means the impact profiles in Figure 14 would need to be stretched out by a comparable value.

Lunar craters formed between one and two billion years ago. The best available ages for large lunar craters formed between 1 and 2 Ga come from studies of the spatial densities of small craters ($D < 1$ km) formed on terrains produced by large craters. The ages derived from these studies assume that the small crater production rate has been constant for the last 3 Gyr and that the large craters Tycho and Copernicus have well defined ages from Apollo samples of ∼0.1 and ∼0.8 Ga (e.g., Wilhelms 1987). If one accepts these conditions, we can assert that there are four $D > 70$ km lunar craters that formed between 0.5 and 2.0 Ga: Copernicus (97 km, 0.8 Ga), King (76 km, 0.99 Ga), Vavilov (99 km; 1.7 ± 0.1 Ga), and Hayn (86 km; 1.7 ± 0.1 Ga; e.g., Wilhelms 1987; Ashley et al. 2011; Hiesinger et al. 2012; Kirchoff et al. 2013). Evidence supporting these ages comes from Grier et al. (2001), who found that King and Vavilov have roughly the same optical maturity as Copernicus. Hayn was not analyzed. Still, given unknowns in the small-body impact flux over the last 3 Gyr, we would argue that, with the possible exception of Copernicus, all of these crater ages are probably uncertain by a few additional hundreds of megayears beyond the formal uncertainty of the fit between model and crater size distributions.

Using the crater scaling law described by Bottke et al. (2016), where a typical projectile striking the lunar surface makes a crater that is 24 times larger than itself, we predict that the projectile size needed to make $D \geqslant 70$–100 km craters was $D \simeq 3$–4 km (see, however, Johnson et al. 2016, for an alternative view on lunar crater scaling laws). In Section 4.2, we estimated that Flora was fully capable of making one of these craters, preferentially within the the first ∼500 Myr after its breakup.

Lunar glass impact spherules. Insights into the last several gigayears of impacts can also be gleaned from studies of dated lunar impact spherules. These glasses are quenched melts that were produced during cratering events on the Moon (e.g., Culler et al. 2000; Zellner & Delano 2015). They are found in some abundance within the regolith samples returned by the Apollo astronauts, and many have been dated using the 40Ar/39Ar system.

Ideally, lunar spherules are a proxy telling us about the impact flux; more impacts of a given age presumably mean more spherules produced and launched around the Moon. The challenging issue is to properly interpret the data given the selection effects (e.g., older glasses destroyed while residing in the regolith; we do not know the volume of spherules produced in a given lunar impact event nor how far they are thrown, etc.;

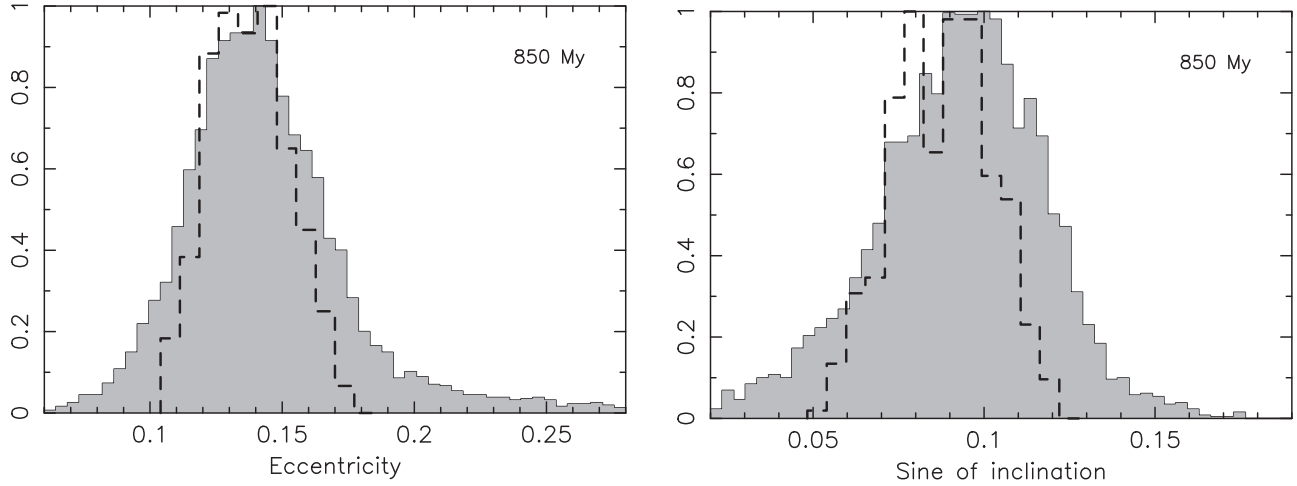

Figure 16. Comparison between the model and observed proper eccentricity (left) and sine of inclination (right) distributions for the Flora family at time 850 Myr. See Figure 15 for additional details, in particular, the initial velocity dispersal of fragments was $v_{ej} = 300$ m s^{-1}. Weak mean motion and secular resonances produce diffusive dynamical effects similar to those seen in our production run with $v_{ej} = 100$ m s^{-1} (Figures 7 and 8).

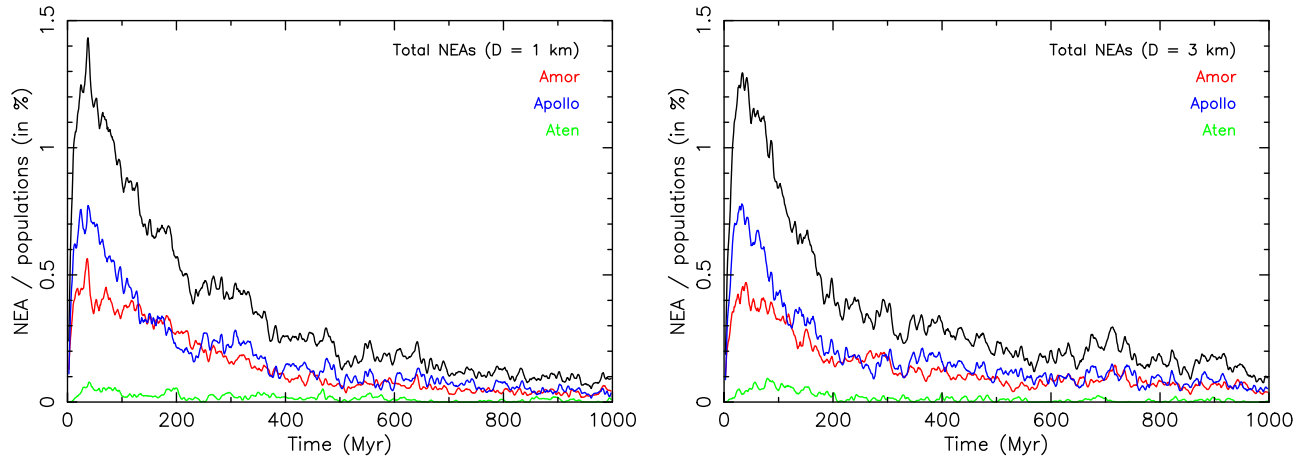

Figure 17. Same as in Figure 12, but now for the simulation with initial ejection velocity of fragments $v_{ej} = 300$ m s^{-1}. Left panel: $D = 1$ km asteroids. Right panel: $D = 3$ km asteroids. Time since the family formation event took place is on the abscissa. The population abundance at the ordinate is expressed as a fraction of the initial population of objects in the Flora family zone (this was 10 000 in our synthetic family). In this case, the initial surge after the family formed is larger due to fragments launched right into the ν_6 resonance, or very close to it.

see Zellner & Delano 2015, for additional details and references). On the more positive side, the age distribution of lunar spherules broadly matches our expectations for how the lunar impact flux has changed over the last 3–4 Ga, and they have made at least one successful prediction (e.g., a change in the impact flux of 0.3–0.4 Ga; Culler et al. 2000; Mazrouei et al. 2017). Accordingly, it makes sense to see what they might be telling us about impacts between 0.5 and 2.0 Ga.

The most recently produced age distribution of lunar spherules comes from Zellner & Delano (2015). They find that age events took place at approximately 0.8 Ga, 1.05 Ga, and 1.6 Ga. The 0.8 Ga event is probably related to the formation of Copernicus, though arguments have been made for an impact spike taking place at that time (Zellner et al. 2009). A compilation of spherule ages by Culler et al. (2000), Levine et al. (2005), Hui et al. (2010), and Norman et al. (2012), which together cover the Apollo 12, 14, 16, and 17 sites, indicates that an increase in impacts starts near 1.6 Ga that lasts 0.4 to 0.7 Ga. In several data sets, there also appears to be a number of ages near 1.2 Ga. Taken at face value, these data would seem to provide putative evidence for a Flora family formation event near 1.5–1.6 Ga or so, with subsequent family member impacts taking place over the subsequent several hundreds of megayears (e.g., Figure 14). With that said, however, these data are fairly murky, and the putative signature of Flora impacts is not pronounced.

Degradation state of lunar craters. Somewhat subtle supporting evidence for a change near 1.6–1.7 Ga may also be found in the degradation state of younger lunar craters Fassett & Thomson (2014). By mapping 0.8–5 km diameter craters on dated lunar maria and characterizing how they gradually slump into a shallower bowl, Fassett & Thomson (2014) found a statistical relationship describing how fast craters degrade at different lunar times. It can be argued their crater breakdown rate is a proxy for the lunar impact flux, with craters collapsing faster when the impact flux is high. As supporting evidence, the Fassett & Thomson (2014) method predicts that crater degradation rates over the last 0.3–0.4 Gyr are much faster than the previous gigayear, results that are consistent with a change in the impact flux near that time (e.g., Culler et al. 2000; Mazrouei et al. 2017).

For their data relevant to the age of Flora family impactors, they found that the degradation rate between 0.5 and 1.7 Ga was higher than that between 1.7 and 2.7 Ga. Thus, a modest inflection point may take place near the predicted age of Flora. As with the impact spherules, though, this interpretation should be treated with considerable caution.

5.2. Origin of the LL Chondrite-like NEOs

Several groups have suggested that the Flora family is a plausible source for the large number of NEO with spectroscopic signatures similar to LL-type ordinary chondrites (e.g., Vernazza et al. 2008; de León et al. 2010; Dunn et al. 2013; Binzel et al. 2015). In quantitative terms, recall that out of $\simeq$1000 $D \geqslant 1$ km NEAs, some 65% are S- or Q-type category objects, of which about 60% have near-infrared signatures compatible with LL-type ordinary chondrites. So, taken altogether, we expect about 400 $D \geqslant 1$ km NEAs to be LL-type compatible. Up to now, the link to the Flora family has made logical sense. The pro side of this argument can be distilled down to the following.

1. Numerous LL-type NEOs are found on orbits consistent with them coming from the innermost region of the asteroid belt.
2. The Flora family is large, it has LL-type spectra, and it is located in the innermost region of the asteroid belt.
3. About 8% of all meteorite falls are LL chondrites, higher than all other classes of falls except L and H chondrites, and as such they likely come from a prominent family located near a good transportation route that can take the bodies to Earth.

As we discuss here, though, our runs suggest that there are substantial cons to this hypothesis as well.

1. The Flora family appears to be >1–1.3 Ga old, it has lost nearly 90% of its kilometer-sized bodies, and it no longer appears capable of producing more than modest quantities of kilometer-sized NEOs via the ν_6 resonance (about 35−50, Section 4.2).
2. The most plausible sources of large quantities of meteorite falls are younger asteroid families or those that have an exceptional breakup history (e.g., Bottke et al. 2005, 2015a). A good example of this is the 470 Ma Gefion family, which is a plausible source of the L chondrites (Nesvorný et al. 2009). A second example is the 1 Ga Rheasilvia cratering event on Vesta, which appears to be a likely source of the HED meteorites (e.g., Marchi et al. 2012, 2014). The Flora family is older than both. It may still be the source of the LL chondrites, but the evidence is more equivocal than previously thought.

As a possibility, we may mention that the Flora-family halo, not accounted for in our $N(1)$ or $N(3)$ calibrations, might slightly increase the true Flora contribution, but perhaps not much. With this said, however, some family, or possibly the inner main-belt background population, has to produce the influx of LL chondrite-like NEOs. One possible source could be the Baptistina family. It has an inner main-belt location, an age <0.3 Ga (e.g., Bottke et al. 2007; Masiero et al. 2012) and possibly the right LL composition (Reddy et al. 2014). A second possibility would be the Hertha family, which is located near the Mars-crossing region in the inner main belt, it has an age near 0.3 Ga, and it has a possible LL-type composition (Dykhuis & Greenberg 2015). These intriguing possibilities set the stage for lots of compelling future work for numerical modelers, observers, and meteoricists.

We thank Joe Masiero for his suggestions that helped to improve the original version of this manuscript. This research was supported by the Czech Science Foundation (grant GA13-01308S). W.F.B.'s and D.N.'s participation was supported by NASAs SSERVI program, the Institute for the Science of Exploration Targets" (ISET), through institute grant number NNA14AB03A.

Appendix
Long-term Orbital Evolution of (8) Flora

The results of our simulations discussed above assumed long-term orbital stability of (8) Flora, the largest member of the Flora family. In particular, in Section 3.1 we constructed our initial Flora family using the current orbit of (8) Flora, assuming it had been stable for over 1 Gyr. While this is arguably a reasonable starting point for our work, in lieu of better information, we explore this issue using numerical simulations in this Appendix.

We first selected the nominal orbit of (8) Flora, as defined on September 2016, and generated 50 clones of its orbit (i.e., clones are test asteroids that have similar but not identical orbits to (8) Flora). All clones were located in the orbit-uncertainty hyper-ellipsoid in the space of equinoctical orbital elements at MJD 57600.0. All needed information was obtained from the `AstDyS` website. We used the `swift` integrator to propagate the orbits of all 51 test asteroids (Flora and 50 clones) in the gravitational field of the planets Mercury through Neptune forward in time for 2 Gyr. Given the large size of this asteroid, we did not apply Yarkovsky/YORP nongravitational thermal forces discussed in Section 3.2. Our integration timestep was three days. We output state vectors of all propagated bodies every 10 kyr. In order to reduce the displayed results, we computed mean orbital elements—semimajor axis, eccentricity, and inclination—over a running 5 Myr wide window, which was slid in 100 kyr increments.

Our results are shown in Figure 18. Many of the clones did not survive the integrated timespan, including the nominal orbit of (8) Flora that was discarded at $\simeq$1.84 Gyr. Most of the 39 destabilized particles were eliminated by approaching within 0.05 au of the Sun. One test asteroid hit Venus. Even the test asteroids that survived 2 Gyr in our simulation showed traces of long-term instability by undergoing a macroscopic random-walk in their mean orbital elements. These survivors were slowly transferred to orbits with slightly smaller mean eccentricities and inclinations, both of which provided Flora with some protection against the mechanisms that would push them into the planet-crossing region.

To understand the source of the long-term orbital instability, we first examined the Lyapunov timescale of (8) Flora and found it was only $\simeq$25 kyr (as reported by `AstDyS`). This short value suggests the clones orbits are indeed chaotic. For Flora, this does not manifest itself in a violent instability seen, for instance, when test bodies are injected into a major mean-motion resonance with Jupiter. Instead, the chaos is weak, or as Milani & Nobili (1992) have coined it, stable. Still, over long timescales, the stable chaos may produce orbital instability, explaining our Figure 18 results.

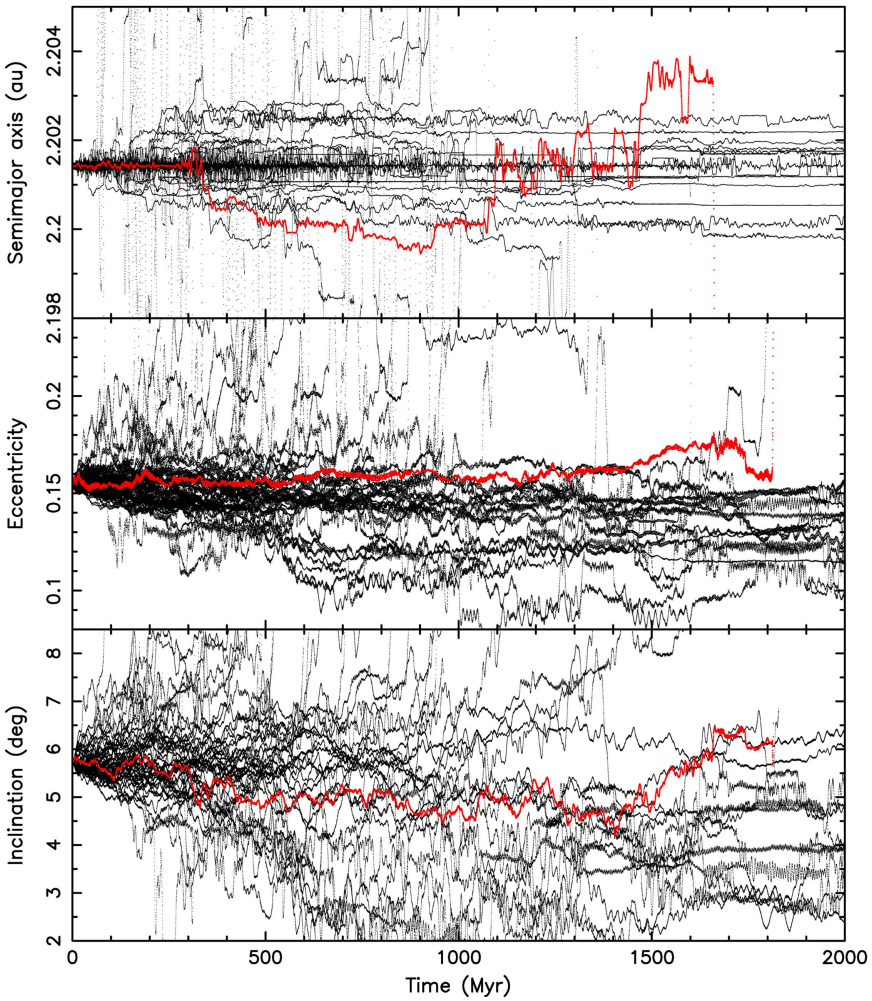

Figure 18. Mean orbital elements of (8) Flora and its close clones: (1) red line for the nominal orbit, (2) black lines for 50 clones all starting from the uncertainty ellipsoid as of the initial epoch MJD 57600.0. The three panels show semimajor axis (top), eccentricity (middle), and inclination (bottom) vs. time. We find that some clones were eliminated before the elapsed time reached 2 Gyr (see Figure 19).

Somewhat surprisingly, we believe that the primary trigger of this long-term instability is not directly related to any resonance but rather is caused by close encounters with Mars. Indeed, while the current osculating perihelion of the orbit of (8) Flora is $\simeq$1.85 au, it becomes as small as $\simeq$1.678 au within the next several hundreds of thousands of years. The reason for this large oscillation is the nearby ν_6 secular resonance (see Figure 2). Over short timescales, the aphelion of Mars becomes as large as $\simeq$1.713 au. While not directly overlapping in the next megayear, the chances of direct close approaches of (8) Flora to Mars are not zero over a timescales of tens to hundreds of megayears.

The probability that Flora's orbit will become unstable as a function of time is shown in Figure 19. In particular, the black line shows the fraction of surviving test asteroids in the simulation, while the gray line shows the fraction of test asteroids remaining in approximate core zone of the Flora family. The core zone is defined by the location of $D \geqslant 3$ km fragments; they have mean semimajor axes in the interval of (2.16, 2.36) au, mean eccentricities in the interval of (0.11, 0.19), and mean sine of inclination values in the interval of (0.06, 0.13). Interestingly, we find that the decay dynamics during the first gigayear of our simulation is somewhat faster than in the second gigayear. This implies that the surviving bodies are slowly seeking more stable niches in orbital space via chaotic diffusion.

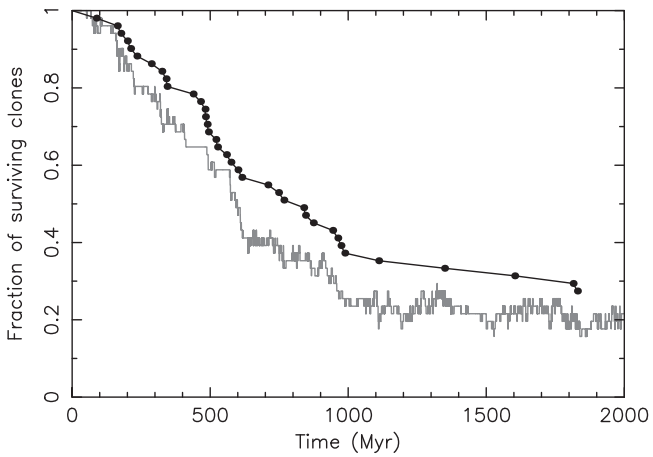

Figure 19. Decay curves from our numerical integration of the orbit of (8) Flora and its 50 clones shown in Figure 18. The black line gives the fraction of test asteroids that remain in the simulation (the symbols highlight epochs when individual clones are eliminated). The gray line shows the fraction of test asteroids that remain in the core zone of the Flora family (see the text).

Our results have several implications. First, the current orbit of (8) Flora is not stable on a gigayear-long timescale. This could suggest that the parent body was on a more stable orbit at

the time of the family-forming event (i.e., modestly smaller eccentricity and/or inclination, or slightly larger semimajor axis) and subsequently evolved to its current location. We find this idea fascinating but hard to prove. A systematic offset between the mean values of these elements seen in the initial data at Figures 7 and 8 may argue in favor of this case. Regardless, we believe that our results in the main text are valid at the zeroth order even if the initial data were modified accordingly.

Second, we find it rather curious that such a large asteroid as (8) Flora, singular in its orbital zone with a diameter of 140 ± 1 km (e.g., Masiero et al. 2011), may become macroscopically unstable via close encounters with Mars. In order to explain this, we hypothesize two scenarios.

In scenario 1, the orbital eccentricity of (8) Flora has been increasing in response to weak resonant phenomena, which in turn lowers its minimum perihelion distance. Consider that the innermost main-belt zone is rich in weak mean-motion resonances with Mars as well as three body resonances (e.g., Morbidelli & Nesvorný 1999; Nesvorný et al. 2002b). Searching for the relevant evolutionary path is beyond the scope of this paper. Another option is that the semimajor axis of (8) Flora is smaller than that of the Flora parent body (which was therefore residing on a more stable orbit). Note that the largest remnant (8) Flora likely represents 50% or less of the mass of the parent body (e.g., Michel et al. 2002). This means that the collective mass of the fragments is larger than the largest remnant. In this situation, an offset of (8) Flora from the semimajor axis of the parent body would not be a surprise. Modeling this possibility, with all of its free parameters, is also beyond the scope of this paper and left for future work.

In scenario 2, Mars' eccentricity has been slowly increasing over time, which in turn would increase Mars' maximum aphelion distance. This scenario may be more plausible than one might think. For example, Laskar et al. (2004) or Laskar (2008) have shown that the motion of terrestrial planets is chaotic, such that over long timescales planetary eccentricities may diffuse to larger values. They have shown that over billions of years, Mars' eccentricity may increase by few times 0.01. If this occurred over the last billion years, major asteroid families like Flora or Nysa/Polana (sometimes called Hertha/New Polana; e.g., Nesvorný et al. 2015) would be more easily destabilized, allowing their family members to reach planet-crossing orbits more readily. A larger Martian eccentricity would also increase the width (and strength) of Mars' mean-motion resonances, which in turn would accelerate the dynamical erosion of the inner main belt (e.g., Morbidelli & Nesvorný 1999).

If the orbit of (8) Flora eventually reaches the planet-crossing region over the next billion years, it will literally become a giant among dwarfs. Consider that the two largest NEOs today are (1036) Ganymed and (433) Eros, with diameters of 34×32 km and 34.4×11.2 km, respectively, while (8) Flora is $\simeq$140 km. The prospective escape of other large asteroids from the main belt (e.g., the dynamical diffusion of large asteroids near the 3:1 mean-motion resonance with Jupiter; see cases described in Guillens et al. 2002 or Vokrouhlický et al. 2016), are still small in comparison to (8) Flora. Our simulations suggest that (8) Flora may become unstable within the next hundreds of megayears. A putative impact on the Earth, roughly a 1.5% chance, would certainly terminate all macroscopic life as we know it.

References

Ashley, J. W., Hawke, B. R., Dicarlo, N., et al. 2011, M&PSA, 74, 5498
Binzel, R. P., Reddy, V., & Dunn, T. L. 2015, in Asteroids IV, ed. P. Michel, F. E. DeMeo, & W. F. Bottke (Tucson, AZ: Univ. Arizona Press), 243
Bottke, W. F., Brož, M., O'Brien, D. P., et al. 2015a, in Asteroids IV, ed. P. Michel, F. E. DeMeo, & W. F. Bottke (Tucson, AZ: Univ. Arizona Press), 243
Bottke, W. F., Durda, D., Nesvorný, D., et al. 2005, in IAU Coll. 197: Dynamics of Populations of Planetary Systems, ed. Z. Knežević & A. Milani, 357
Bottke, W. F., & Greenberg, R. 1993, GeoRL, 20, 879
Bottke, W. F., Morbidelli, A., Jedicke, R., et al. 2002a, Icar, 156, 399
Bottke, W. F., Nesvorný, D., Grimm, R. E., Morbidelli, A., & O'Brien, D. P. 2006a, Natur, 439, 821
Bottke, W. F., Nolan, M. C., Greenberg, R., & Kolvoord, R. A. 1994, Icar, 107, 255
Bottke, W. F., Vokrouhlicky, D., Ghent, B., et al. 2016, in Lunar and Planetary Science Conf. 47, 2036
Bottke, W. F., Vokrouhlický, D., & Nesvorný, D. 2007, Natur, 449, 48
Bottke, W. F., Vokrouhlický, D., Rubincam, D. P., & Brož, M. 2002b, in Asteroids III, ed. W. F. Bottke et al. (Tucson, AZ: Univ. Arizona Press), 395
Bottke, W. F., Vokrouhlický, D., Rubincam, D. P., & Nesvorný, D. 2006b, AREPS, 34, 157
Bottke, W. F., Vokrouhlický, D., Walsh, K. J., et al. 2015b, Icar, 247, 191
Breiter, S., Nesvorný, D., & Vokrouhlický, D. 2005, AJ, 130, 1267
Brouwer, D. 1950, AJ, 55, 162
Brouwer, D. 1951, AJ, 56, 9
Brož, M., & Morbidelli, A. 2013, Icar, 223, 844
Brož, M., Morbidelli, A., Bottke, W. F., et al. 2013, A&A, 551, A117
Čapek, D., & Vokrouhlický, D. 2004, Icar, 172, 526
Carruba, V., & Nesvorný, D. 2016, MNRAS, 457, 1332
Carry, B. 2012, P&SS, 73, 98
Chapman, C. R. 1996, M&PS, 31, 699
Chapman, C. R., Paolicchi, P., Zappala, V., Binzel, R. P., & Bell, J. F. 1989, in Asteroids II, ed. R. P. Binzel, T. Gehrels, & M. S. Matthews (Tucson, AZ: Univ. Arizona Press), 386
Cotto-Figueroa, D., Statler, T. S., Richardson, D. C., & Tanga, P. 2015, ApJ, 803, 25
Culler, T. S., Becker, T. A., Muller, R. A., & Renne, P. R. 2000, Sci, 287, 1785
de León, J., Licandro, J., Serra-Ricart, M., Pinilla-Alonso, N., & Campins, H. 2010, A&A, 517, A23
Delbò, M., dell'Oro, A., Harris, A. W., Mottola, S., & Mueller, M. 2007, Icar, 190, 236
Dunn, T. L., Burbine, T. H., Bottke, W. F., & Clark, J. P. 2013, Icar, 222, 273
Dykhuis, M. J., & Greenberg, R. 2015, Icar, 252, 199
Dykhuis, M. J., Molnar, L., Van Kooten, S. J., & Greenberg, R. 2014, Icar, 243, 111
Dykhuis, M. J., Molnar, L. A., Gates, C. J., et al. 2016, Icar, 267, 174
Fassett, C. I., & Thomson, B. J. 2014, JGRE, 119, 2255
Ghent, R. R., Hayne, P. O., Bandfield, J. L., et al. 2014, Geo, 42, 1059
Giblin, I., Martelli, G., Farinella, P., et al. 1998, Icar, 134, 77
Gladman, B. J., Migliorini, F., Morbidelli, A., et al. 1997, Sci, 277, 197
Gradie, J. C., Chapman, C. R., & Williams, J. G. 1979, in Asteroids, ed. T. Gehrels (Tucson, AZ: Univ. Arizona Press), 359
Granvik, M., Morbidelli, A., Jedicke, R., et al. 2016, Natur, 530, 303
Granvik, M., Morbidelli, A., Vokrouhlický, D., et al. 2017, A&A, 598, A52
Greenberg, R. 1982, AJ, 87, 184
Greenberg, R., Nolan, M. C., Bottke, W. F., Jr., Kolvoord, R. A., & Veverka, J. 1994, Icar, 107, 84
Grier, J. A., McEwen, A. S., Lucey, P. G., Milazzo, M., & Strom, R. G. 2001, JGR, 106, 32847
Guillens, S. A., Vieira Martins, R., & Gomes, R. S. 2002, AJ, 124, 2322
Hanuš, J., Brož, M., Durech, J., et al. 2013, A&A, 559, A134
Harris, A. W., & D'Abramo, G. 2015, Icar, 257, 302
Hiesinger, H., van der Bogert, C. H., Pasckert, J. H., et al. 2012, JGRE, 117, E00H10
Hirayama, K. 1918, AJ, 31, 185
Hirayama, K. 1919, AOTok, 8, 52
Hirayama, K. 1922, JaJAG, 1, 55
Hirayama, K. 1928, JaJAG, 5, 137
Holsapple, K., Giblin, I., Housen, K., Nakamura, A., & Ryan, E. 2002, in Asteroids III, ed. W. F. Bottke, Jr. et al. (Tucson, AZ: Univ. Arizona Press), 443
Hui, S., Norman, M. D., & Jourdan, F. 2010, in Proc. 9th Australian Space Science Conf., ed. W. Short & I. Cairns (Sydney: National Space Society of Australia Ltd), 43, http://www.nssa.com.au/9assc/downloads/9assc-proceedings-lores.pdf

Ito, T., & Malhotra, R. 2010, A&A, 519, A63
JeongAhn, Y., & Malhotra, R. 2014, Icar, 229, 236
JeongAhn, Y., & Malhotra, R. 2015, Icar, 262, 140
Johnson, B. C., Collins, G. S., Minton, D. A., et al. 2016, Icar, 271, 350
Kirchoff, M. R., Chapman, C. R., Marchi, S., et al. 2013, Icar, 225, 325
Knežević, Z., & Milani, A. 2000, CeMDA, 78, 17
Knežević, Z., Milani, A., Farinella, P., Froeschle, C., & Froeschle, C. 1991, Icar, 93, 316
Kozai, Y. 1979, in Asteroids, ed. T. Gehrels (Tucson, AZ: Univ. Arizona Press), 334
Kryszczyńska, A. 2013, A&A, 551, A102
Kryszczyńska, A., Colas, F., Polińska, M., et al. 2012, A&A, 546, A72
Laskar, J. 2008, Icar, 196, 1
Laskar, J., Correia, A. C. M., Gastineau, M., et al. 2004, Icar, 170, 343
Levine, J., Becker, T. A., Muller, R. A., & Renne, P. R. 2005, GeoRL, 32, L15201
Lindsay, F. N., Delaney, J. S., Herzog, G. F., et al. 2015, E&PSL, 413, 208
Marchi, S., Bottke, W. F., O'Brien, D. P., et al. 2014, P&SS, 103, 96
Marchi, S., Chapman, C. R., Barnoiun, O. S., Richardson, J. R., & Vincent, J.-B. 2015, in Asteroids IV, ed. P. Michel, F. E. DeMeo, & W. F. Bottke (Tucson, AZ: Univ. Arizona Press), 725
Marchi, S., McSween, H. Y., O'Brien, D. P., et al. 2012, Sci, 336, 690
Masiero, J. R., DeMeo, F. E., Kasuga, T., & Parker, A. H. 2015, in Asteroids IV, ed. P. Michel, F. E. DeMeo, & W. F. Bottke (Tucson, AZ: Univ. Arizona Press), 323
Masiero, J. R., Mainzer, A. K., Bauer, J. M., et al. 2013, ApJ, 770, 7
Masiero, J. R., Mainzer, A. K., Grav, T., et al. 2011, ApJ, 741, 68
Masiero, J. R., Mainzer, A. K., Grav, T., Bauer, J. M., & Jedicke, R. 2012, ApJ, 759, 14
Mazrouei, S., Ghent, S., Bottke, W. F., et al. 2017, NatAs, in press
McKinnon, W. B., Zahnle, K. J., Ivanov, B. A., & Melosh, H. J. 1997, in Venus II: Geology, Geophysics, Atmosphere, and Solar Wind Environment, ed. S. W. Bougher, D. M. Hunten, & R. J. Phillips (Tucson, AZ: Univ. Arizona Press), 969
Michel, P., Tanga, P., Benz, W., & Richardson, D. C. 2002, Icar, 160, 10
Milani, A., Cellino, A., Knežević, Z., et al. 2014, Icar, 239, 46
Milani, A., & Knežević, Z. 1992, Icar, 98, 211
Milani, A., & Knežević, Z. 1994, Icar, 107, 219
Milani, A., & Nobili, A. M. 1992, Natur, 357, 569
Morbidelli, A., & Gladman, B. 1998, M&PS, 33, 999
Morbidelli, A., & Henrard, J. 1991, CeMDA, 51, 131
Morbidelli, A., & Nesvorný, D. 1999, Icar, 139, 295
Nesvorný, D., Bottke, W. F., Dones, L., & Levison, H. F. 2002a, Natur, 417, 720
Nesvorný, D., Brož, M., & Carruba, V. 2015, in Asteroids IV, ed. P. Michel, F. E. DeMeo, & W. F. Bottke (Tucson, AZ: Univ. Arizona Press), 297
Nesvorný, D., & Morbidelli, A. 1998, AJ, 116, 3029
Nesvorný, D., Morbidelli, A., Vokrouhlický, D., Bottke, W. F., & Brož, M. 2002b, Icar, 157, 155
Nesvorný, D., Vokrouhlický, D., Bottke, W. F., Gladman, B., & Häggström, T. 2007, Icar, 188, 400
Nesvorný, D., Vokrouhlický, D., Morbidelli, A., & Bottke, W. F. 2009, Icar, 200, 698
Norman, M. D., Adena, K. J. D., & Christy, A. G. 2012, AuJES, 59, 291
O'Brien, D. P., Greenberg, R., & Richardson, J. E. 2006, Icar, 183, 79
Parker, A., Ivezić, Ž., Jurić, M., et al. 2008, Icar, 198, 138
Pravec, P., Harris, A. W., Kušnirák, P., Galád, A., & Hornoch, K. 2012, Icar, 221, 365
Pravec, P., Harris, A. W., Vokrouhlický, D., et al. 2008, Icar, 197, 497
Reddy, V., Sanchez, J. A., Bottke, W. F., et al. 2014, Icar, 237, 116
Rubincam, D. P. 2000, Icar, 148, 2
Scheeres, D. J., Britt, D., Carry, B., & Holsapple, K. A. 2015, in Asteroids IV, ed. P. Michel, F. E. DeMeo, & W. F. Bottke (Tucson, AZ: Univ. Arizona Press), 745
Spray, J. G. 2017, Earth Impact Database, Planetary and Space Science Centre (Univ. New Brunswick)
Statler, T. S. 2009, Icar, 202, 502
Valsecchi, G. B., Carusi, A., Knezevic, Z., Kresak, L., & Williams, J. G. 1989, in Asteroids II, ed. R. P. Binzel, T. Gehrels, & M. S. Matthews (Tucson, AZ: Univ. Arizona Press), 368
Vernazza, P., Binzel, R. P., Thomas, C. A., et al. 2008, Natur, 454, 858
Vokrouhlický, D., Bottke, W. F., Chesley, S. R., Scheeres, D. J., & Statler, T. S. 2015, in Asteroids IV, ed. P. Michel, F. E. DeMeo, & W. F. Bottke (Tucson, AZ: Univ. Arizona Press), 509
Vokrouhlický, D., Breiter, S., Nesvorný, D., & Bottke, W. F. 2007, Icar, 191, 636
Vokrouhlický, D., Brož, M., Bottke, W. F., Nesvorný, D., & Morbidelli, A. 2006a, Icar, 182, 118
Vokrouhlický, D., Brož, M., Morbidelli, A., et al. 2006b, Icar, 182, 92
Vokrouhlický, D., Milani, A., & Chesley, S. R. 2000, Icar, 148, 118
Vokrouhlický, D., Nesvorný, D., & Bottke, W. F. 2006c, Icar, 184, 1
Vokrouhlický, D., & Čapek, D. 2002, Icar, 159, 449
Vokrouhlický, D., Ďurech, J., Pravec, P., et al. 2016, A&A, 585, A56
Vraštil, J., & Vokrouhlický, D. 2015, A&A, 579, A14
Wilhelms, D. E. 1987, The Geologic History of the Moon, US Geological Survey Professional Paper 1348, https://pubs.er.usgs.gov/publication/pp1348
Zappalà, V., Bendjoya, P., Cellino, A., Farinella, P., & Froeschlé, C. 1995, Icar, 116, 291
Zappalà, V., Cellino, A., Farinella, P., & Knežević, Z. 1990, AJ, 100, 2030
Zappalà, V., Cellino, A., Farinella, P., & Milani, A. 1994, AJ, 107, 772
Zappalà, V., Cellino, A., Gladman, B. J., Manley, S., & Migliorini, F. 1998, Icar, 134, 176
Zellner, N. E. B., & Delano, J. W. 2015, GeCoA, 161, 203
Zellner, N. E. B., Delano, J. W., Swindle, T. D., et al. 2009, GeCoA, 73, 4590